102 pages

STRUCTURAL CHARACTERIZATION AND GAS REACTIONS OF SMALL METAL PARTICLES BY HIGH-RESOLUTION, IN-SITU TEM AND TED

Annual Report

for the Period
January 1, 1984 - December 31, 1984

Submitted to

National Aeronautics and Space Administration
Ames Research Center
Moffett Field, CA 94305

Computational Chemistry and Aerodynamics Branch
Dr. Jim Arnold, Chief
Dr. Helmut Poppa, Technical Monitor

Grant No.:
NCC 2-283

Prepared by

ELORET INSTITUTE
1178 Maraschino Drive
Sunnyvale, CA 94087
(Phone: (408) 730-8422)
K. Heinemann, President and Principal Investigator

STRUCTURAL CHARACTERIZATION AND GAS REACTIONS OF SMALL METAL PARTICLES BY HIGH-RESOLUTION, IN-SITU TED AND TEM

ABSTRACT

The existing in-situ TEM facility was improved by adding a separately pumped mini-specimen chamber. The chamber contains wire-evaporation sources for three metals and a specimen heater for moderate substrate temperatures. A sample introduction device was constructed, installed, and tested, facilitating rapid introduction of a specimen into the mini-chamber while maintaining the background pressure in that chamber in the 10(-9) millibar range.

Small particles and clusters of Pd, grown by deposition from the vapor phase in an in-situ TEM facility on amorphous and crystalline support films of alumina and on ultra-thin carbon films, were analyzed by conventional high- resolution TEM and image analysis in terms of detectability, number density, and size distribution. The smallest particles that could be detected and counted contained no more than 6 atoms; size determinations could be made for particles >1 nm in diameter. The influence of various oxygen plasma treatments, annealing treatments, and of increasing the substrate temperature during deposition was investigated.

The TEM technique was employed to demonstrate that under otherwise identical conditions the lattice parameter of Pd particles in the 1-2 nm size range and supported in random orientation on ex-situ prepared mica films is expanded by some 3% when compared to 5 nm size particles. It is believed that this expansion is neither a "small-particle diffraction effect" nor due to pseudomorphism, but that it is due to a annealing-induced transformation of the small as-deposited particles with predominantly composite crystal structures into larger particles with true f.c.c. structure and thus inherently smaller lattice parameter.

I. IMPROVEMENT OF IN-SITU TEM FACILITY

The existing in-situ TEM facility, based on a Siemens Elmiskop 101 transmission electron microscope with a large, custom stainless steel specimen chamber <1>, was modified to include a specimen introduction system and a minichamber with improved vacuum at the site of the specimen. Fig.1 shows a true-scale cross-sectional schematic drawing of the center portion of the regular custom chamber with mini-chamber and front end of the specimen introduction system. In this drawing, items (1) to (3) show the bottom of the existing custom stainless steel chamber, the upper pole piece of the objective lens, and a vacuum seal between the two, respectively. Item (4) is the specimen table which glides on the pole piece (2) upon x-y movement with the specimen drives which are made of uhv-compatible components and with bellows feedthroughs and are located inside the existing stainless steel chamber (10). Items (6) and (7) are lower and upper parts of the minichamber, which is held within the specimen table (4) with a conical insert (5) which can be adjusted in z-direction (parallel to the electron beam). The lower part of the chamber has the contours of the bore in the pole piece, but is mounted without touching it or the aperture body (see Fig.2), and contains a 600 micron hole for exit of the electron beam. The upper part (7) of the minichamber contains a conically shaped bore which seats the upper portion (5) of the

specimen holder. When the specimen holder is inserted for microscopy, as shown in Fig.1, the lower portion of the specimen holder (11) rests on the lower inside ledge of the minichamber. When the specimen is being removed by upward movement of the specimen holder assembly (50)/(52), the two wires (9) engage in piece (11) and lift it. Upward motion of the specimen holder (50) with (11) is achieved by lateral motion of rod (54); while this rod is moved to the left, piece (52), which is connected with pieces (50) and rod (54) by hinges, glides over the contour of piece (8) with the lower hinge point moving straight upward. This upward motion finally turns into a sideward motion after the lower part (11) of the specimen holder has cleared the minichamber. At that time, most of the rod (54) is already retracted into the tube (31). Further retraction conceals finally the entire specimen holder in this tube, which can then be retracted entirely through the airlock (not shown) to the outside. Part (52) contains a coaxial hole for the electron beam, and part (50) contains a 600 micron aperture to reduce the conductance between the main chamber (at 1* 10(-8) mbar) and the minichamber (10(-10) mbar pressure range). When the sample is inserted for microscopy, parts (52) and (50) are disengaged to avoid vibrations from the transfer rod to be transmitted to the specimen via direct contact with the minichamber. When the sample is removed, the now created 12 mm DIA hole into the minichamber is closed with a gravity-operated mini-flapper valve (not

shown).

Part (41) shows the pumping line for the minichamber. A bellows connector isolates the pumping section in terms of vibrations from the minichamber. In the vertical portion of part (41) a custom, pre-calibrated nude ionization gauge (not shown) is installed to allow accurate pressure readings at the site of the specimen. All parts are made of 304 stainless steel, except for part (11) which is made of tantalum. Baking of the minichamber is achieved by
(a) the filament of the ionization gauge;
(b) operating (underheated) a titanium sublimator pump mounted at the right side of the bellows at part (41);
(c) and operating underheated simultaneously all three wire source evaporators mounted in the space below the top plate of the minichamber (7).

At present, a vacuum at the site of the specimen of 2*10(-9) mbar has been obtained with a LN2-trapped oil diffusion pump operated with Santovac 5 fluid. Calculations indicate that a vacuum in the mid (-10) range should be obtained with a well baked pump. Indications are that the present limitations are due to the pump; and arrangements are underway to replace the diffusion pump with an ion pump.

Operations of the microscope have shown that the base image

resolution of the original in-situ TEM facility has not been affected by the introduction of the mini- chamber and the sample introduction system. The x-y lateral movement of the specimen, severely restricted by the small size of the apertures in parts (6) and (50), seems nevertheless sufficient for most practical applications.

IN-SITU TEM EVIDENCE OF LATTICE EXPANSION OF VERY SMALL PALLADIUM PARTICLES ON SINGLE CRYSTAL SUBSTRATES

Small clusters of palladium (1-2 nm size range) were deposited at room temperature inside a controlled-vacuum specimen chamber (10(-8) millibar background pressure) onto muscovite mica substrate surfaces. After electron micrographs and diffraction patterns of the randomly oriented deposit had been taken under conditions minimizing electron beam exposure, small sample areas were flash-heated with the electron beam to induce particle coalescence to some 5 nm mean particle size. Photoplates containing diffraction patterns, taken at the same specimen areas before and after particle sintering under otherwise identical conditions, were analyzed by photo-densitometry, using corresponding mica reflections as relative internal standards. Assuming that the Pd lattice parameter of particles in the 5 nm size range is that of bulk palladium, the lattice parameter of particles in the 1.5 nm mean size range is increased by (2.9 +- 0.3)%. The results were discussed in the light of recent findings of a significant lattice parameter increase of small Pd particles epitaxially grown on MgO <2> and of electron diffraction calculations of very small metal aggregates <3>. It was determined that the observed lattice expansion is not due to pseudomorphism, which was the predominant mechanism in ref. <2>, and "apparent" lattice expansion <3> has been ruled out by careful choice of the

particle sizes involved. It is, instead, believed that the lattice expansion is primarily due to a transformation of the 1.5 nm as-deposited Pd particles with predominantly composite crystal structure <4, 5, 6> into larger particles with true f.c.c. structure and with inherently smaller lattice parameter <4>.

A preprint of a paper submitted for publication covering these results <8> is attached as APPENDIX 1 to this report. Reference <3>, which has also been submitted for publication within the present grant-year, is included as APPENDIX 2.

PREPARATION AND ANALYSIS OF PARTICULATE METAL DEPOSITS

Small particles and clusters of Pd were grown by deposition from the vapor phase under uhv conditions. Amorphous and crystalline support films of alumina and ultra-thin amorphous carbon films were used as substrate materials. The growth of the metal deposit was monitored in-situ by scanning transmission diffraction of energy-filtered 100 keV electrons and high-resolution TEM analysis performed in a separate instrument. It was established, however, by in-situ TEM that the transfer of specimens in this case did not unduly affect the size and distribution of the deposit particles, as had earlier been found for the case of Pd/MgO in-situ depositions <7>.

It was found that the cleanliness, stoicheometry, crystallinity, and structural perfection of the support surface play an essential role in determining the crystalline perfection and structure of the particles. For example, Pd/alumina deposits could be greatly affected by prior exposure of the substrate film to an oxygen plasma which presumably oxidized the alumina substrate to perfect stoicheometry. In that case, fine Pd deposits appeared independent of the crystal structure of the alumina support (amorphous, gamma/delta, or alpha). On not treated alpha alumina surfaces, the deposit particles were much smaller and exhibited a higher number density. In spite of the

oxygen plasma treatment, Pd deposits on carbon films were quite different (higher number densities, higher sticking coefficient) from those on alumina substrates.

The smallest clusters reproducibly prepared contained no more than 6 atoms; but size determinations below 1 nm average particle diameter are very problematic with conventional TEM. Pd particles grown on carbon supports feature a (probably) impurity-stabilized mosaic structure.

A preprint of a paper on this subject <9>, submitted for publication, is attached as APPENDIX 3 to this report.

REFERENCES

<1> K. Heinemann and T. Osaka, J. Crystal Growth 59, 1982, 485.

<2> K. Heinemann, T. Osaka, H. Poppa, and M. Avalos-Borja, J. Catalysis 83, 1983, 61.

<3> P. Gallezot, M. Avalos-Borja, H. Poppa, and K. Heinemann, submitted for publication (preprint included as APPENDIX 2).

<4> C.Y. Yang, J. Crystal Growth 47, 1979, 274.

<5> M.J. Yacaman, K. Heinemann, and H. Poppa CRC Critical Reviews in Solid State and Mat. Sci., 1981, 243.

<6> K. Heinemann, M.J. Yacaman, C.Y. Yang, and H. Poppa, J. Crystal Growth 47, 1979, 177 and 187.

<7> K. Heinemann, T. Osaka, and H. Poppa, Ultramicroscopy 12, 1983, 9.

<8> K. Heinemann and H. Poppa, "In-situ TEM Evidence of Lattice Expansion of Very Small Supported Pd Particles," submitted for publication (preprint included as APPENDIX 1).

<9> H. Poppa, D. Moorhead, and K. Heinemann, "Preparation and Analysis of Particulate Metal Deposits," submitted for publication (preprint included as APPENDIX 3).

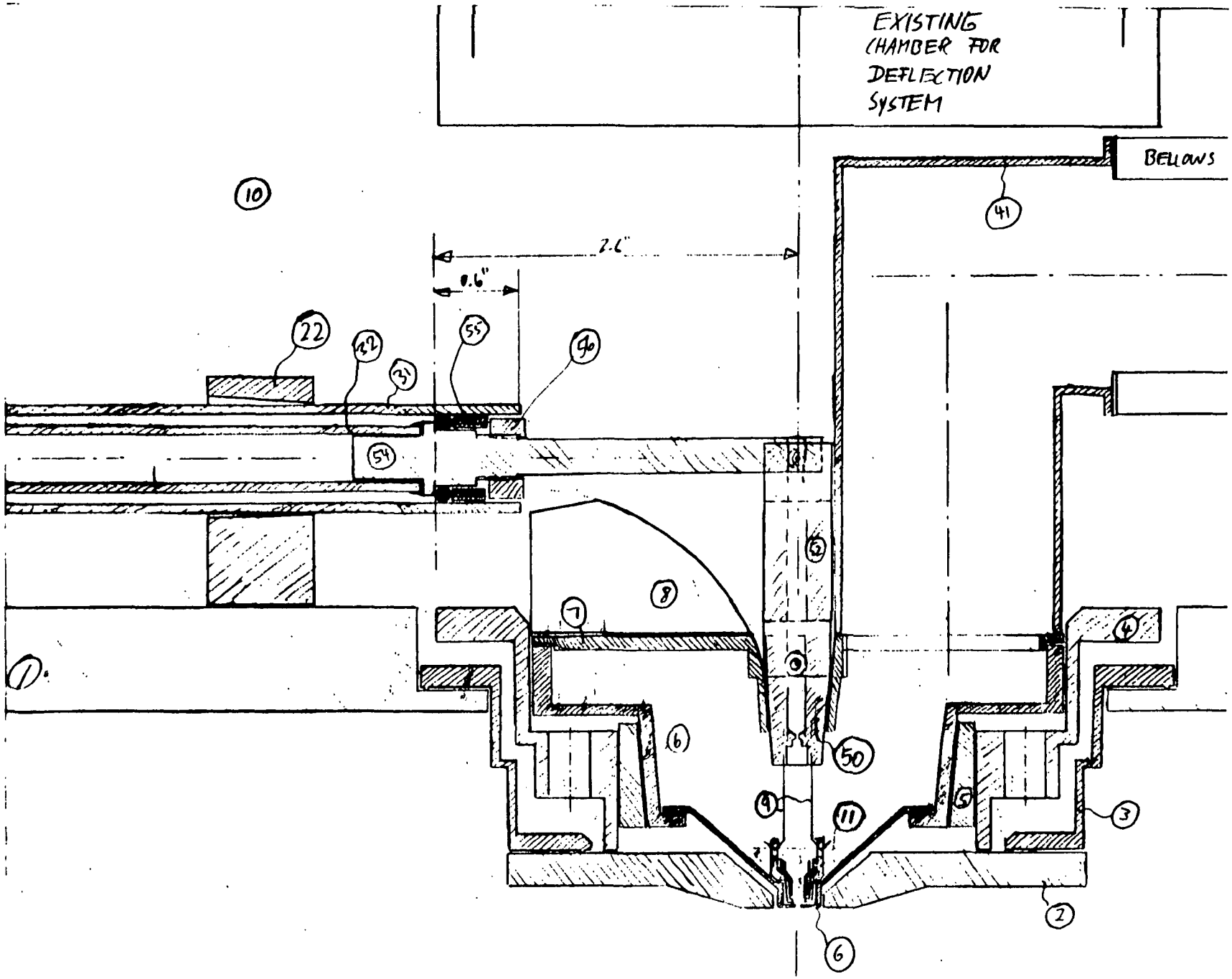

FIG. 1

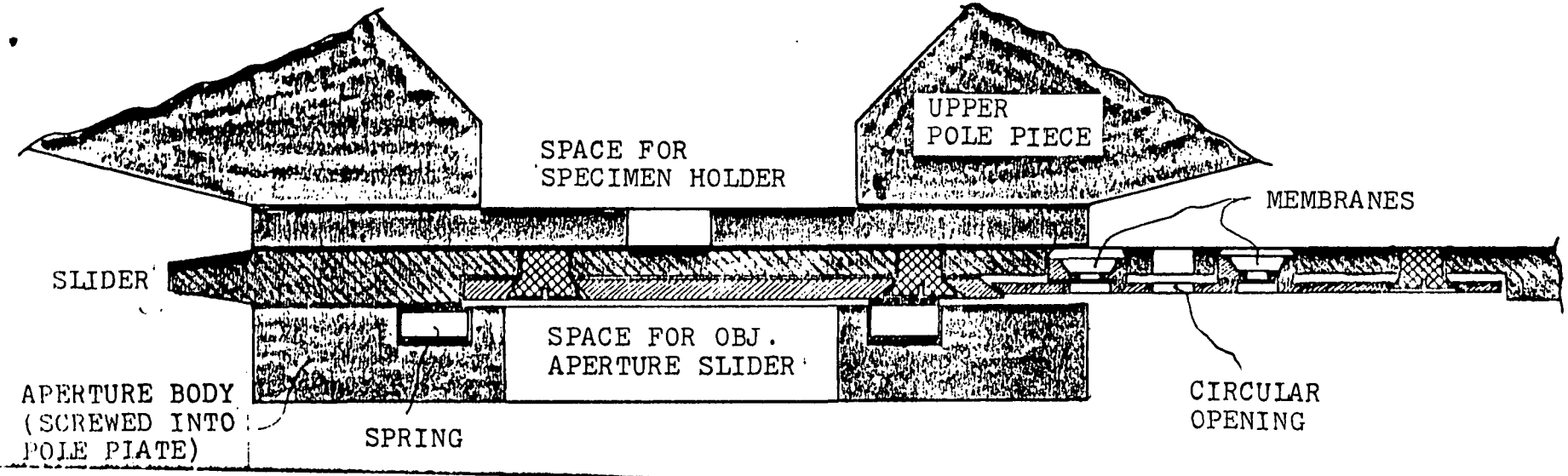

FIG. 2

APPENDIX 1

IN-SITU TEM EVIDENCE OF LATTICE EXPANSION OF VERY SMALL SUPPORTED PALLADIUM PARTICLES

K. Heinemann* and H. Poppa

Stanford/NASA Joint Institute for Surface and Microstructure Research, Moffett Field, CA 94035

* Eloret Institute, 1178 Maraschino Drive, Sunnyvale, CA 94087, U.S.A.

ABSTRACT

A direct, in-situ TEM technique was employed to demonstrate that under otherwise identical conditions the lattice parameter of palladium particles in the 1-2 nm size range (supported in random orientation on ex-situ prepared muscovite mica) is expanded by (2.9 + 0.2)% when compared to particles of 5 nm mean size in which case the lattice parameter is believed to have reached the bulk value. The expansion is not due to pseudomorphism and is considered to only secondarily be a size effect. It is instead believed to be primarily due to a transformation of the 1.5 nm as-deposited Pd particles with predominantly composite crystal structures into larger particles with true f.c.c. structure and with inherently smaller lattice parameter.

INTRODUCTION

The increased interest in structure-sensitive catalysts has revitalized research efforts on the structure of very small particles. The smaller the particles, the more difficult the task of determining such vital characteristics as the crystal structure, morphology, and lattice parameter, because most of the methods used to determine these parameters are based on scattering of X-rays or electrons, which becomes increasingly difficult to detect and assess with decreasing particle size. Whereas for particles larger than about 3 nm excellent high-resolution TEM methods exist, such as direct imaging of lattice planes (e.g., (1, 2)) and various methods of dark field imaging (e.g., (2-5)), with which shape, structure, and morphology of small particles can be determined, comparatively very little has been published on particles less than 1.5 nm in size.

In the size range up to 1.5 nm, the ratio of surface- to bulk coordinated atoms in the clusters is very high, which often gives rise to dramatically different catalytic behavior of such small particles compared to bulk material, and which can alter the crystal structure and the lattice parameter of these particles. It has, for example, been suggested that the initial growth of f.c.c. crystals occurs as multiply twinned particles (MTP's) (6-7), and earlier work in our laboratory has resulted in evidence that the crystal structure of twinned particles is (slightly) different from f.c.c., e.g., body-centered orthorhombic for decahedral particles

and rhombohedral for icosahedral particles (8, 5). This in turn implies that the 'lattice parameter,' if deduced from low-order diffraction rings that are indexed as if the structure were f.c.c., is also different from the bulk material. For the case of decahedral and icosahedral particles, a reduction of the packing density, when compared to the f.c.c. packing density, by 2.28% and 7.06% has been calculated (8), respectively, giving rise to a commensurate 'lattice expansion' for these MTP's. Other investigators have also reported lattice parameter changes of small particles, and a broad spectrum of results, from moderate lattice contraction to substantial expansion has been reported for various metal/ substrate systems and experimental conditions (9 - 18).

We have recently published findings of lattice expansion for small particles of palladium deposited in-situ under controlled vacuum conditions onto MgO (19). This expansion ranged from 2-4% for the smallest detected particles, which were in the 1 to 1.5 nm size range, and Anton and Poppa (17) reported expansion of small Pd particles deposited at elevated temperatures onto carbon, mica, and alumina substrates. Whereas most of this earlier work involved a high degree of epitaxy (19), where pseudomorphism as major explanation for the lattice expansion could not be excluded (or other questions, such as impurity stabilized composite crystals, were left unanswered), no experiment has been reported where the lattice parameter of small particles was determined in-situ at the same substrate area, before and after manupulation of the size of the particles such as by local e-beam heating induced sintering of

small into larger particles. It is the subject of the present paper to further quantify the phenomenon of lattice expansion of small metal particles by employing such a technique that optimally excludes any ambiguities stemming from different treatment of the evaluated samples.

EXPERIMENTAL AND RESULTS

Palladium was deposited from a wire source installed in a custom stainless-steel specimen chamber fitted to a Siemens Elmiskop 101 TEM converted for in-situ experimentation (19, 20). A total nominal thickness of 0.5 nm of palladium was deposited at a rate of 0.1 nm/min (assuming unity sticking coefficient) at room temperature onto muscovite mica specimens prepared ex-situ by thermally induced cleavage from a bulk mica sample (21). During deposition and the subsequent coalescence treatment, the background pressure was maintained below $2*10^{-8}$ mbar. After taking micrographs and selected-area diffraction patterns of the as-prepared deposit (Fig.1a), the imaged specimen area was exposed to a mild flash-electron beam to induce short local heating and concomitant particle coalescence. Microscopy at the same reference area (Fig.1b) as well as at other areas that had not been affected by the flash heating was then resumed. In addition to a sharpening of the diffraction lines, commensurate with the larger crystallite size (5 nm after flash heating vs. 1.5 nm before) due to less Scherrer- broadening (22, 23), minor texturing of the originally completely random deposit was noted, similar to earlier findings for gold on alpha-alumina where thermally induced epitaxy of orignally randomly oriented deposit particles was reported (24). Further experiments checked by TEM and TED at the same reference areas included annealing up to 250 C and exposure to hydrogen and CO at 250 C for 10 min at $5*10^{-5}$ mbar partial pressure of the respective gas. Neither of these latter treatments had a notable

effect on the TEM or TED results, i.e., on the shape, number density, location, and degree of epitaxy of the particles, and we therefore show only the final status of the reference specimen area in Fig.1c.

The diffraction patterns were evaluated by light optical densitometry. Using the Pd (111) reflections of the 5 nm particles as a standard, i.e., assuming that these reflections correspond to the bulk lattice parameter of 0.38893 nm for palladium (i.e., d(Pd 111)=0.2246 nm), we determined the d-spacing for a characteristic pair of mica reflections contained in the same densitometer trace (Fig.2, curve A, 0.1266 nm). We then used this spacing as a calibration standard for the densitometer trace of the SAD taken before particle coalescence had been induced (Fig.2, curve B) and determined the palladium d-spacings accordingly. Utmost care was used to always scan pairs of SAD patterns in the same directions in order to eliminate any errors stemming from substrate film bending. The results indicate a consistent 2.9% increase of the lattice parameter of the 1.5 nm Pd-particles. The error margin in the determination of the lattice parameters was 0.2%. The exposure of the 5 nm Pd particles to hydrogen at elevated temperature did not affect the lattice parameter, which suggests that the particles had not been notably oxidized. However, the exposure to CO did slightly expand the lattice of the 5 nm particles. (Whereas all other lattice expansion reported here occurred uniform, the expansion due to CO exposure was non-uniform: it was found to be 0.8% for 111 planes, 0.6% for 100 planes, and within the error margin no

expansion was found for 110 planes.)

DISCUSSION

The finding of 2.9% expansion of the lattice of small Pd particles seems qualitatively in agreement with our earlier results on MgO (19) as well as with Anton and Poppa's results (17). Turkevich et al. (18) report a lattice parameter increase averaging 1.5% over the bulk parameter for Pd presumably supported on carbon. Their conclusion is based on TEM lattice images of Pd particles upwards of 2 nm in size. They report that the lattice parameters measured for Pd varied substantially with particle size, and they found no lattice expansion in similar experiments with Pt particles. Takayanagi et al. (9) presented a micrograph of Pd islands deposited at 350 C on MgO showing moire fringes. They measured the moire fringe spacings to be 2.5 nm and suggest that they are of the 200 type. Under these assumptions, their islands would have the bulk Pd lattice parameter. However, considering the <100> direction indicated in their figure (Fig.7 of (9)) and the epitaxial relations Pd<100>//MgO<100> and Pd(100)//MgO(100) (9,19), the direction of the moire fringes suggests that they are of the 220 type, instead. In this case, a 2.2% expansion would result. This result is actually unexpected, because it refers to quite large particles (5 - 10 nm size range), well within the size range where for the present case of randomly oriented Pd particles on mica we

are already assuming the bulk lattice parameter. We therefore tend to explain their result as due to pseudomorphism, which is consistent with our earlier interpretation of our own results for Pd/MgO (19). This, in turn, renders our present results not confirmed by, but rather separate from these earlier results (19, 9), necessitating an explanation different from pseudomorphism in this case.

Our present results contrast with earlier results obtained in our laboratory for the case of gold on mica, where evaluation of (i) the imaged substrate lattice planes, (ii)the directions and spacings of (rotational) Au/mica moiré fringes, and (iii) the angles between particle and substrate directions determined by the particle contours and the direction of the imaged lattice planes, led to the conclusion that the lattice parameter of the gold deposit was actually contracted (by about 1%, decreasing for increasing particle size) when compared to the bulk parameter of gold. This result was averaged from a number of micrographs such as Fig.6 in (25). It was obtained in spite of the circumstance that (i) the gold particles were considerably larger (10 - 50 nm) than the Pd particles in the present case, and that (ii) the substrate lattice parameter was actually larger, which means that the lattice misfit actually increased rather than decreased in that case. Mays et al. (11) found similar shrinkage for gold on carbon. Boswell (12) earlier measured lattice shrinkage of almost 2% in gold particles of some 2 nm in diameter. The results were explained in terms of surface stress, which is increased for small

particles due to the high surface- to- volume ratio. Palmberg and Rhodin (26) refined this explanation in terms of enhanced surface valency. The findings for gold are further complemented by an evaluation of earlier TED and TEM results obtained in our laboratory for gold on sapphire, where an originally fully random deposit was epitaxially realigned (24) by local electron beam heating similar to the method used in the present report (see Fig.3). Densitometry of the SAD patterns of that experiment yields a modest lattice contraction of 0.6% in well textured regions (Fig.3b) that had experienced moderate flash heating temperatures (stage d of Fig.2 in ref.(24)) and up to 0.95% in those regions that had been exposed to relatively high flash heating temperatures and showed perfect epitaxy (Fig.3c). Contrary to the present results, epitaxial realignment occurred in that case without substantial increase of the mean particle dimension (of about 7 nm). The lattice contraction can, therefore, in that case not be explained as a particle size effect. Instead, it could be attributed either to pseudomorphic influence or to the circumstance that a high fraction of the as-deposited particles were composite crystals, including icosahedra, in which case the 220-like reflections would have been expected to appear at a smaller diameter in the SAD patterns (27, 8) and would thus have simulated an expanded lattice of the 110 planes that were used for this measurement. The results show indeed that during the process of thermally induced epitaxy (24), the majority of the particles auto-sintered into single crystal particles, now having true f.c.c. structure. This can be deduced from the much larger number of

particles showing uniform diffraction contrast within the entire particle outline (Fig.3b and c), rather than the "fragmented" diffraction contrast (Fig.3a) which is characteristic for composite particles (including decahedral and icosahedral particles) (5, 8, 28). Hence, the lattice has appeared shrunk. Although the first of these two possible explanations (pseudomorphism) for the observed lattice "shrinkage" in the experiment of ref. (24) does conform with the Au(111)//α-alumina($1\bar{1}02$) epitaxial orientation (Au<110>//α-alumina<$\bar{1}012$>) that had been induced, we lend more credence to the latter explanation that involves the transformation of composite particles into f.c.c. particles.

The combined findings for gold and palladium on various substrates indicate then the following two basic mechanisms by which the lattice parameter of small, clean particles can be influenced: (i) a pseudomorphic influence that is described by an interaction between the metal and the support and may, if the misfit is negative (metal lattice smaller than support lattice) lead to an expansion, and (ii) an influence of the high surface-to-volume ratio of the particles, generally leading to contraction. To these one can add two more factors that can lead to an apparent change of the lattice parameter: (iii) a crystallographic effect, such as a change from icosahedral (or otherwise polyhedral or composite) structure to f.c.c. crystal structure during particle growth, which would appear to indicate a larger lattice parameter for the small particles (8), and (iv) an pure diffraction effect (not further discussed here), where the

multiplication of a Scherrer- broadened scattering pattern (with peaks at the exact Bragg positions) with the rapidly decreasing atomic scattering function (resulting in the experimentally observed diffraction intensity pattern) leads to the appearance of a lattice expansion (29). Mechanism (i) is likely to explain lattice expansion results for Pd/MgO (19, 9, 17), for which system the metal/support interaction is known to be considerable (30) and may include oxygen bridges between the metal atoms in the substrate and the particles (31). This is unlikely, however, if the particles are positioned in a random orientation on the substrate. The results for gold on mica, as reported here in conjunction with our earlier work (25), are most likely explained with mechanism (ii). However, The present results for Pd/mica seem to not fall in either of these categories: absence of epitaxy for the as-deposited particles rules out (i), and the observation of lattice expansion instead of contraction is in general conflict with (ii). On the other hand, mechanism (iv) is also ruled out, because the mean particle size (1.5 nm) is in the region where the apparent change in lattice parameter (29) is inherently small. If no other chemical effects have influenced the particles (the hydrogen exposure experiment has rendered unlikely an influence by residual oxygen), we submit mechanism (iii) as the most probable explanation for the lattice expansion observed for 1.5 nm Pd particles essentially randomly oriented on (possibly not clean) mica. Although we have, due to the small size of the particles, no TEM proof of the composite (including icosahedral) crystal structure of the 1.5 nm Pd particles, the 5 nm Pd particles certainly do not look multiply

twinned (Fig.1b), and the result obtained for Au/α-alumina upon flash heating (Fig.3), although obtained for considerably larger particles, can be used to prove the validity of the process of a transformation from composite (including icosahedral) to f.c.c. crystal structure in general. Mechanism (iii) would also explain the lattice expansion observed by Anton and Poppa (17) for Pd/C and Pd/mica, and it is interesting to note that a "high degree of disorder" by strong broadening of the diffraction lines was found in that work, even for "nearly continuous" Pd films. These discontinuities of mosiac-like particle morphologies (32) could well be agglomerizations of very small multiply twinned particles with lattice parameters that, if expressed in f.c.c. terminology, are expanded (8).

CONCLUSIONS

The lattice parameter of 1.5 nm Pd particles, deposited in random orientation on mica, is expanded by (2.9 + 0.2)%. Out of several possible mechanisms, this result was explained as most likely due to a transformation from composite particles, including those having an icosahedral crystal structure (5, 8, 27, 28), believed to having been the prevailing structure of the as-deposited Pd particles (31), into the bulk f.c.c. crystal structure during local e-beam annealing, the former having an expanded lattice (by about 5%) when compared to the latter (8). The validity of such a transformation with concomitant apparent lattice parameter shrinkage was demonstrated for the example Au/ -alumina. Because of the lack of epitaxy (most likely due to the low degree of cleanliness of the mica support), pseudomorphism is unlikely to explain the present Pd/mica results; and physical effects due to the high surface-to-volume ratio in small particles would explain lattice contraction and could also be ruled out, therefore. The Pd/mica lattice expansion could also not be explained on the basis of an 'apparent' lattice parameter increase expected for very small particles (29).

We conducted in-situ gas exposure tests showing that background pressure oxygen exposure of the Pd/mica particles had not affected the lattice parameter results. However, other contaminants cannot be entirely ruled out as having influenced these results, considering the circumstance that our in-situ experiments were

REFERENCES

(1) K. Heinemann and H. Poppa, Appl. Phys. Lett. 20, 122, 1972.

(2) L.D. Marks and D.J. Smith, J. Crystal Growth 54, 425 and 433, 1981, J. Microscopy 130, 249, 1982.

(3) M.J. Yacaman and T. Ocana, Phys. Status Solidi (a) 42, 571, 1977

(4) M.J. Yacaman, K. Heinemann, and H. Poppa, CRC Critical Reviews in Solid State and Mat. Sci., (1981) p. 243.

(5) K. Heinemann, M.J. Yacaman, C.Y. Yang, and H. Poppa, J. Crystal Growth 47, 177 and 187, 1979.

(6) S. Ino and S. Ogawa, in: Advances in Epitaxy and Endotaxy, ed. H.G. Schneider and V. Ruth, VEB Deutscher Verlag fuer Grundstoffindustrie, Leipzig, 1971, ch.4

(7) El Gillet and M. Gillet, J. Cryst. Growth 13/14, 212, 1972.

(8) C.Y. Yang, J. Crystal Growth 47, 274, 1979.

(9) K. Takayanagi, K. Yagi, and G. Honjo, Thin Solid Films 48, 137, 1978.

(10) P. Gallezot, Surf. Sci. 106, 459, 1981.

(11) C.W. Mays, J.S. Vermaak, and D. Kuhlmann-Wilsdorf, Surf. Sci. 12, 134, 1968.

(12) F.W.C. Boswell, Proceed. Phys. Soc. London Sect. A64, 465, 1951.

(13) J. Woltersdorf, A.S. Nepijko, and E. Pippel, Surf. Sci. 106, 64, 1981.

(14) A. Yokozeki, J. Chem. Phys. 68, 3766, 1978.

(15) J.J. Burton and G.J. Jura, J. Phys. Chem. 71, 1937, 1967.

(16) P.A. Tick and A.F. Witt, Surf. Sci. 26, 165, 1971.

(17) R. Anton and H. Poppa, Proceed. 10th Int. Congr. EM, Hamburg, 1982, Vol.2 pp. 509 and 511.

(18) J. Turkevitch, L.L. Ban, and J.H. Wall, in "Perspectives in Catalysis in Commemoration of Jons Jacob Berzelius" (R. Larsson, Ed.), p. 59, Univ. of Lund, Sweden, 1979.

(19) K. Heinemann, T. Osaka, H. Poppa, and M. Avalos-Borja, J. Catalysis 83, 61, 1983.

(20) K. Heinemann and T. Osaka, J. Cryst. Growth 59, 485, 1982.

(21) E.H. Lee, Ph.D. thesis, Stanford University, 1974.

(22) P. Scherrer, Goettinger Nachrichten 2, 98, 1918.

(23) E. Bauer, in "Elektronenbeugung," Verlag Moderne Industrie, Muenchen, 1958.

(24) K. Heinemann, H.K. Kim, and H. Poppa, J. Vac. Sci. Technol. 16, 622, 1979.

(25) H. Poppa, K. Heinemann, and A.G. Elliot, J. Vac. Sci. Technol. 8, 471, 1971.

(26) P.W. Palmberg and T.N. Rhodin, J. Chem. Phys. 49, 134, 1968.

(27) C.Y. Yang, M.J. Yacaman, and K. Heinemann, J.

Cryst. Growth 47, 283, 1979.

(28) C.Y. Yang, K. Heinemann, M.J. Yacaman, and H. Poppa, Thin Solid Films 58,163, 1979.

(29) P. Gallezot, M. Avalos-Borja, H. Poppa, and K. Heinemann, submitted for publication.

(30) G.C. Bond, Metal Support and Additive Effects in Catalysis, B. Imelik et al., edts., Elsevier Publ. Co., Amsterdam, 1982.

(31) G.C. Bond, 3rd Int. Symp. on Small Particles and Inorg. Clusters, Hamburg 1984, paper 06.

FIGURE CAPTIONS

Fig.1. Pd/mica, in-situ deposited at RT and $2*10^{-8}$ mbar, same specimen area; left: as deposited; center: after e-beam flash-heating to obtain particle coalescence; right: after H2 and subsequent CO treatment, each for 15 min at 250 C and $5*10^{-5}$ mbar.

Fig.2. Densitometer traces for Pd/mica with 5 nm and 1.5 nm mean particle size (curves A and B, corresponding to Fig.1b and a, respectively).

Fig.3. Au/α-alumina, in-situ deposited at 650 C and e-beam flash-heated (24), showing an area 10 μm (left), 6 μm (center), and 2 μm (right) away from the center of the flash-heated zone.

limited to 2*10 mbar background pressure and that the ex-situ prepared mica surfaces used in these experiments might be carbon covered.

ACKNOWLEDGEMENTS

Thanks are due to Dr. Miguel Avalos-Borja for contributions in the TEM work leading to Fig.1, and to Mr. J.G. Heinemann for performing the densitometry measurements. Support to Eloret Institute by NASA-Ames (Grant NCC2-283) and by Alcoa Foundation is greatfully acknowledged.

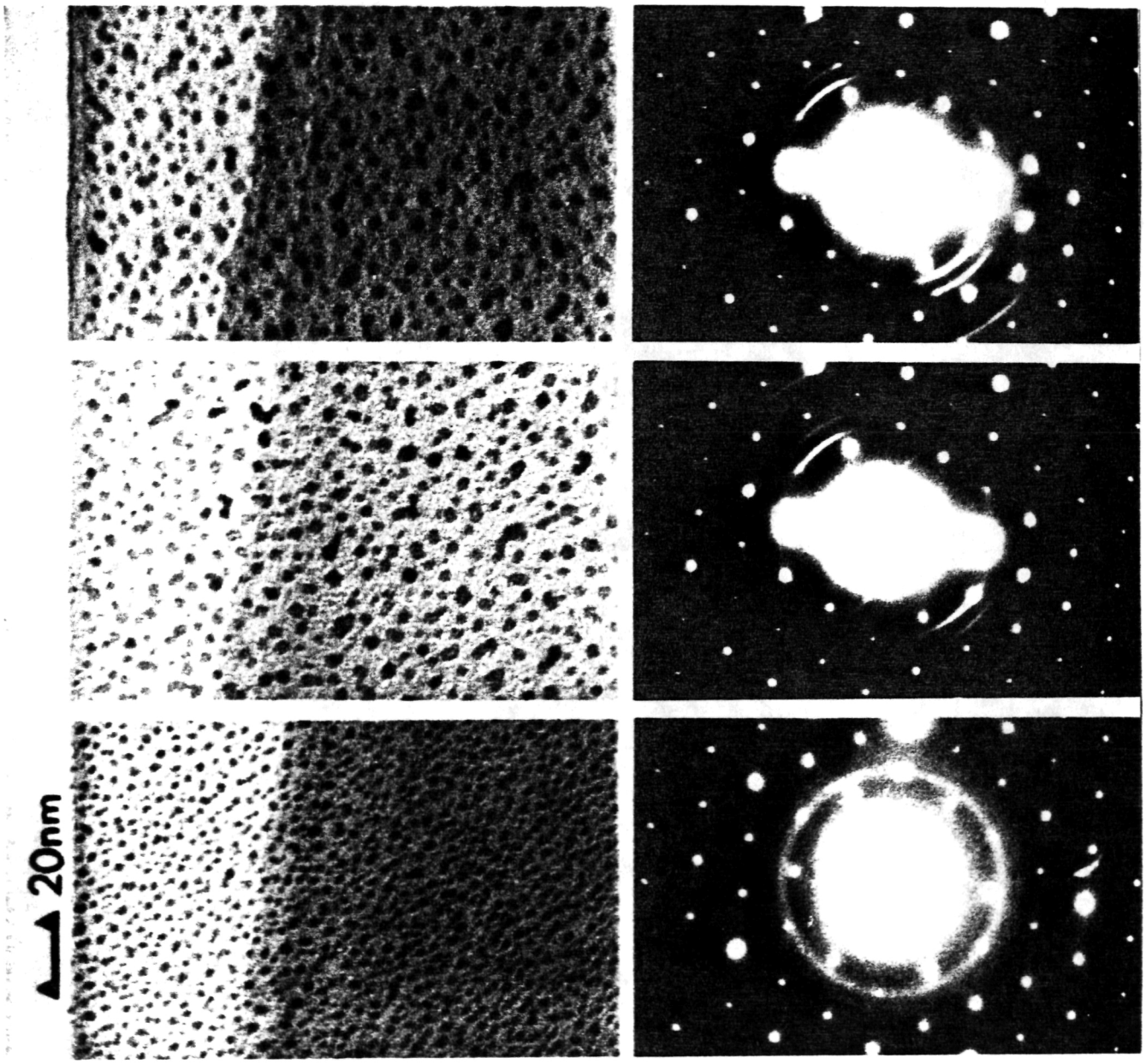

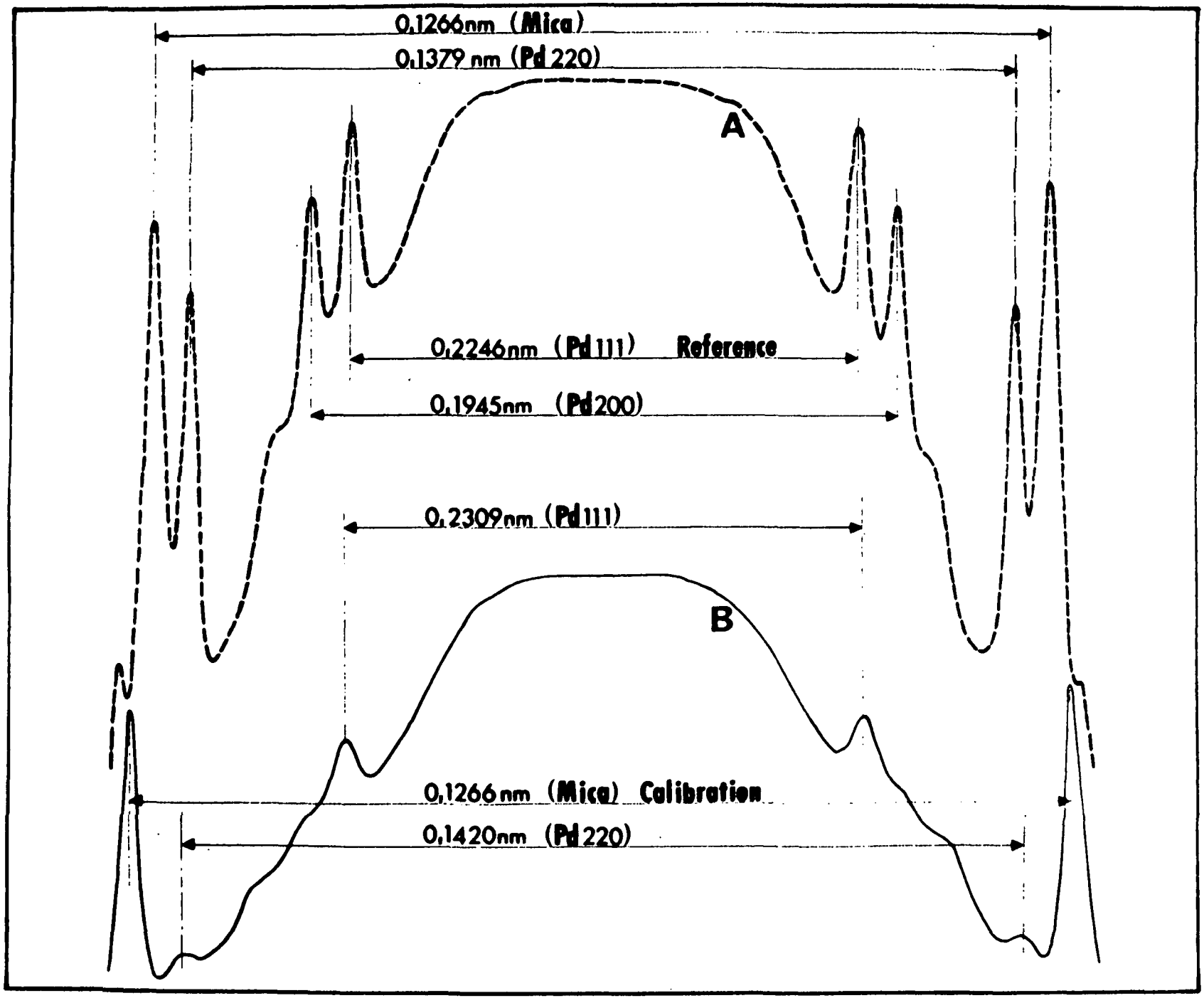
0,1266nm (Mica)
0,1379 nm (Pd 220)
A
0,2246nm (Pd 111) Reference
0,1945nm (Pd 200)
0,2309nm (Pd 111)
B
0,1266 nm (Mica) Calibration
0,1420nm (Pd 220)

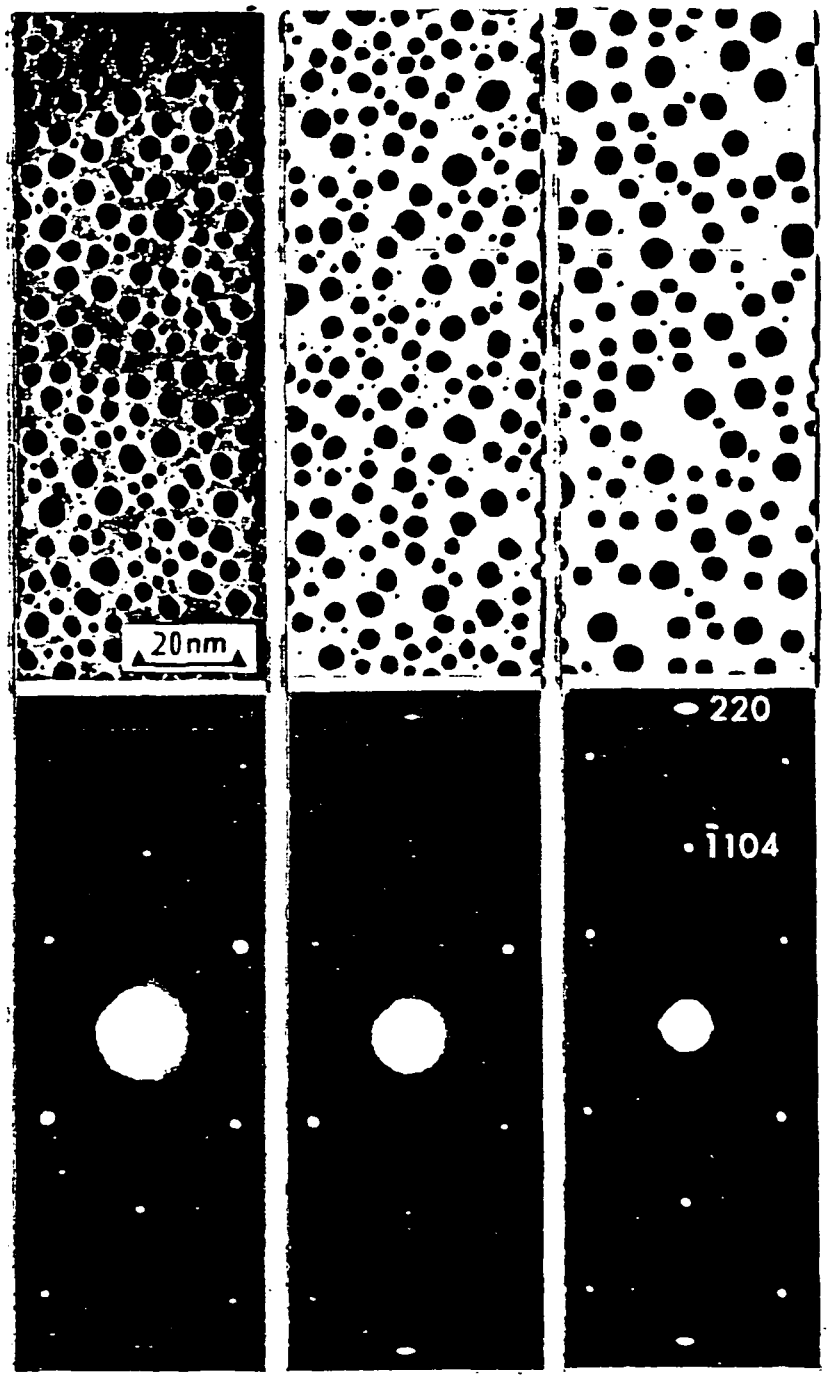

APPENDIX 2

STRUCTURE AND MORPHOLOGY CHARACTERIZATION OF NANOMETER-SIZE METAL AGGREGATES BY ELECTRON SCATTEREING PATTERNS

P. Gallezot*, M. Avalos-Borja**, H. Poppa

Stanford/NASA Joint Institute for Surface and Microstructure Research

NASA-Ames Research Center

Moffet Field, CA 94035, U.S.A.

and

K. Heinemann

ELORET Institute

1178 Maraschino Drive

Sunnyvale, CA 94087

* Permanent address: Institut de Recherches sur la Catalyse, CNRS, 69626 Villeurbanne, France.

** Permanent Adress: Instituto de Fisica, UNAM, Apdo. P. # 877, Ensenada, B.C.N., Mexico.

SUMMARY

Diffraction intensity patterns were calculated for nanometer-size, perfectly structured fcc particles in various orientations and shapes, using the kinematical theory of electron diffraction and bulk interatomic distances. For perfectly epitaxially aligned particles, a shift of the diffraction peak positions toward lower k-values ($k = \sin\theta/\lambda$) was found. This shift increases with decreasing particle size and is explained by the multiplication of a Scherrer-broadened intensity peak at perfect Bragg-position with a rapidly decreasing atomic scattering function. It erroneously gives the impression of a lattice expansion. If the particle orientation is textured or random, a similar particle size-dependent apparent change in lattice parameter exists. It is, however, in this case in part also due to the superposition of the Scherrer-broadened 111 and 200 diffraction rings. The two effects combined give the impression of a lattice expansion if the number of atoms in the particles is less than 20 or larger than 70, and of a slight lattice contraction ($\lesssim$1%) if the clusters consist of 25 to 50 atoms. It was, furthermore, shown that the electron scattering pattern is also influenced by the morphology of the aggregates.

The results suggest that extreme care must be used in the interpretation of electron diffraction patterns of very small particles. What may seem to be a change in the lattice parameter of the particles may in fact only be a diffraction effect, and

computer simulation of diffraction at model particles may be required for a more unambiguous determination of the lattice parameter.

INTRODUCTION

The characterization of the crystallographic structure and morphology of small particles ($\leq$ 2nm) is difficult. TEM imaging techniques give information only on the projected size of the particles and, due to Scherrer-broadening, electron diffraction patterns do not exhibit sharp rings or spots that would allow a straightforward determination of the aggregate's structure. However, electron scattering patterns (SP) can still be used in various ways to study the structure and morphology of small particles, such as (I) by comparison of experimental SP's with patterns calculated for model particles, whereby the model is changed until the best fit is obtained; (II) by evaluation of Fourier transformed scattered intensities (radial distribution function) in terms of interatomic distances and the coordination numbers; (III) by comparison of experimental radial distribution functions (RDF) with the radial distribution (RD) calculated from the atomic coordinates of model aggregates, a procedure from which information on the morphology of aggregates can be obtained. Although these approaches have been known for a long time (1-3), they have not been applied systematically to the study of small metal particles. In this work, we will discuss only the first approach in detail, emphasizing the particular features of electron diffraction patterns of very small aggregates and analyzing to what extent information on the structure, morphology and orientation of the particles can be obtained from such patterns. Particular attention was placed on apparent changes in the position of the

diffraction peaks for the case of small particles, as compared to the peak positions expected for bulk materials under the assumption that the atoms in the small particles maintain bulk interatomic distances. Substrate effects are not considered in this work.

METHOD OF CALCULATION

All the calculations of scattering patterns were carried out with the following assumptions: (a) the kinematical theory of electron diffraction applies for aggregates smaller than 2 - 3nm; (b) the atoms maintain the regular f.c.c. structure, and the interatomic distances are the same as in the bulk metal; and (c) all aggregates used in any one calculation have the same size and shape. Actual calculations were carried out for palladium.

In most cases the particles were assumed to have spherical shapes, i.e., all atoms contained in a sphere of given radius were included for the calculations. Their atom coordinates were calculated using the bulk lattice parameter of 0.38898 nm for Pd. Several particle sizes were assumed, ranging from 6 to 1464-atom clusters. In addition, some other morphologies were used, like platelets or prisms.

The intensity of the electron beam scattered by the aggregates was calculated for 3 particular conditions:

(A) The particles are uniformly oriented with respect to the beam and to other particles (epitaxial deposits).

All particles were considered to be identical in size, shape, and orientation with respect to the imaging beam. The intensity scattered from the sample is then given by summing the scattering amplitudes from the different atoms, and by then multiplying this sum with its complex conjugate value (4,5):

$$I = f_A^2 \left| \sum_{m=1}^{N} e^{(2\pi i/\lambda)(\vec{s} - \vec{s}_o)\vec{r}_m} \right|^2 \qquad (1)$$

where N is the number of atoms, λ the electron wavelength, $\vec{s}_o$ the unit vector in the direction of the incident beam, $\vec{s}$ the unit vector in the direction of observation, $\vec{r}_m$ the position of atom m with respect to a given origin, and f_A the electron scattering amplitude for element A. Values of f_A were taken from the International Tables for X-ray Crystallography.

(B) The particles are in fully random orientation, i.e., the aggregates are allowed to take all possible orientations in space. In this case, eq. (1) is simplified to the well known Debye scattering equation (4):

$$I(s) = f_A^2 \sum_{m=1}^{N} \sum_{n=1}^{N} \frac{\sin(4\pi k r_{m,n})}{4\pi k r_{m,n}}$$

where $r_{m,n}$ is the distance between atoms m and n.

(C) The particle zone axis is parallel to the incident beam, but the particles are in random azimuthal orientation.

The computation was carried out by first calculating the diffraction intensity and then integrating this function on a circle of constant k ($k = \sin\theta/\lambda$), for the range of k values of interest.

RESULTS AND DISCUSSION

1. Apparent Change in Lattice Parameter

1.1 Oriented Aggregates.

Equation (1) indicates that the intensity distribution is formed by multiplying an atomic scattering contribution (f_A^2) with an interference function. The interference function produces diffraction maxima with positions at the expected bulk k values and with all major peaks having the same intensity at the Bragg positions (see Fig.1a) which is a calculation for a 13-atom cluster). However, when multiplied with the rapidly decreasing f_A^2 function (Fig.1a), the expected decrease of the amplitude of higher order peaks is combined with a shift in the peak positions towards lower k values, which gives the impression of larger d spacings. This shift is more pronounced for low-order peaks and for the broader scattering curve profiles that are obtained when the number of atoms is very small, i.e., when appreciable Scherrer-broadening is present. In practice, this effect of "apparent lattice expansion" is only significant for particle sizes of the order of 2 nm or less.

Fig. 2 shows some examples of typical diffraction patterns calculated for clusters with 6 atoms (octahedron), 13 (cuboctahedron), 55 (cuboctahedron), and with 976 atoms (sphere), all aggregates being in <101> orientation. As expected, the peaks

sharper and the details between the peaks (forbidden peaks) weaken when the cluster size increases. From calculations of the positions of the peak maxima, the apparent lattice parameter, corresponding to the displaced peak positions, was derived. This was done separately for the 111 and 200 peaks. In Fig. 3, the change in lattice parameter was plotted as a function of the number of atoms in spherical aggregates of increasing size (see also Tab. 1, col. 3 and 4). The apparent change is substantial if the particles are small, and it is barely noticeable for spherical particles larger than about 3 nm in diameter (consisting of more than 1000 atoms). The change in the 111 peak position is larger than for the 200 peak (under otherwise identical conditions), which is due to the steeper slope of the atomic scattereing function for the 111 beam.

The 'usual' approach for deducing information about possible changes of the lattice parameter is to use the measured peak positions in diffraction patterns from small particles, with substrate diffraction spots or rings as internal calibration standards. However, the above results indicate that this might lead to erroneous conclusions if the particles are very small, since some apparent lattice expansion is expected even if the atoms are assumed to remain in their bulk positions. A correct analysis of electron diffraction patterns of epitaxially oriented small particles would therefore require cancellation of the effect of the atomic scattering factor by dividing the experimental scattering pattern by $f_A^2(k)$, prior to the actual analysis of the peak position.

1.2 Randomly Oriented Aggregates

Figure 4 shows a three dimensional view of the electron scattering intensities of randomly oriented spherical aggregates containing 6, 13, 55 and 976 Pd atoms. The corresponding radial intensity profiles I(k) are given in Fig. 5. Smaller aggregates do not exhibit the usual set of diffraction lines expected of f.c.c. crystals, but they exhibit a smaller number of wide bands instead. The first band is located in the reciprocal space region of the combined 111 and 200 reflections. As the number of atoms in the particles increases, the 200-line begins to appear as a faint shoulder (Fig. 5, 135-atom curve). The 111 and 200 reflections then split into separate peaks for spherical particles larger than about 2 nm in diameter.

The lattice constant of an fcc crystal is often deduced, using the Bragg law, from the position of the maximum of the first line, assuming that to be the 111 reflection. This procedure obviously leads to erroneous conclusions with regard to lattice expansion or contraction if the particles are so small that the 111 and 200 reflections are not yet separated. Table I (last column) and Fig. 6 (dash-dotted curve) give the apparent change of lattice constant with respect to the bulk value. An apparent expansion of the lattice constant is observed for very small aggregates (<15 atoms) and for particles containing more than 70 atoms, whereas a small apparent contraction would result for particles between these size limits. Unlike the case of epitaxially oriented particles,

dividing the experimental scattering curve by $f_A^2(k)$ before applying the Bragg law does not eliminate the apparent change of lattice parameter in this case, but it can in fact result in an apparent lattice contraction for aggregates smaller than about 2 nm. This 'contraction' computes to as much as 3.6% or 2.9% for aggregates containing 19 or 43 atoms, respectively. Therefore, unlike the case of epitaxially oriented crystals, for the case of randomly oriented particles the real lattice constant cannot be directly derived from the maximum of the first reflection, since for small particles, the ambiguity stemming from superposition of 111 and 200 reflection intensities must be dealt with in addition to the ambiguity stemming from the multiplication of Scherrer-broadened intensity patterns with the scattering amplitude. More accurate information can only be obtained by Fourier transforming the scattering patterns and evaluating the resulting radial distribution function.

One also has to be careful when deducing lattice parameter changes for small model aggregates with different shapes. When the shape of the particles is especially anisotropic, the scattering curve can be quite different from that of small spherical aggregates containing the same number of atoms, or from that of bulk crystals. For example, randomly oriented flat aggregates with two stacked 100 layers containing 81 atoms (Fig. 7a), give a scattering curve which exhibits two peaks at k = 2.04 and 2.56 nm^{-1}, whereas the normal positions of the 111 and 200 reflections would be at 2.23 and 2.57nm^{-1}, respectively. Although the second peak is

close to the bulk value for a 200 reflection, the first peak, assumed to be a 111 reflection, would indicate a 9.3% lattice expansion. On the other hand, a particle consisting of two (111) layers (90 atoms, see Fig. 7b), shows only one low-order peak, i.e., a 111 peak at k = 2.20 nm , indicating an apparent 1.2% lattice expansion.

1.3 Particles in Random Azimuthal Orientation

This case falls between the epitaxial and the random cases described above. The <101> common zone axis was the only example calculated, because it produces the same type of diffraction rings as in the case of fully random orientations, and because a method of distinguishing between the two cases was of interest. The profiles are very similar in shape to those calculated for fully randomly oriented particles (Fig. 5). The apparent change in lattice parameter, as deduced from the 111 peak position, is, however, slightly different and is included in Fig. 6 (dash curve) and Tab. I (col. 5). A method of distinguishing between the two cases might be to consider the intensity ratio between the first peak (usually considered the 111 peak) and the second peak (or the 311 peak, if resolved). This ratio (Table II) shows consistently higher values for particles in azimuthally random <101> orientation when compared to the case of fully randomly oriented particles. In this case, as for fully randomly oriented particles, the exact lattice parameter can also not be recovered by simply dividing the

calculated (or experimental) diffraction intensity curve by f_A^2.

2. Structure and Morphology Information

Information on the particle structure and morphology can be obtained by comparing the calculated scattering pattern with an experimental SP. Whereas in principle a number of models can account for the same general appearance of a scattering pattern, most of these models can be eliminated if the particle size is known from independent measurements, such as TEM images (which may be a very difficult or even impossible task in cases where the particles are composites of smaller units -- impurity stabilized (9) or multiply twinned (8)). An example is given in Fig. 9 for the case of randomly oriented particles having a circular appearance in the TEM image, and measuring 2.4 nm in diameter. If a spherical particle modell is assumed, the 111 and 200 diffraction lines are clearly separated (Fig. 9a); but they are not at all separated if the particles -- having essentially the same projected size -- are assumed to have the shape of hexagonal 111 prisms (5 atoms along the edges of the base hexagon) with three stacked (111) planes (Fig. 9b).

The comparison of experimental and calculated diffraction intensity patterns can be particularly useful when the particles exhibit a marked shape- anisotropy. For example, if the aggregates are known to be very thin, 'wetting' the support, the SP would have a very particular profile which permits the characterization of such 'rafts,' which have recently been claimed to exist (6). Furthermore, 100 and 111 rafts exhibit very different scattering

patterns as is evident when comparing Fig. 7a with Fig. 7b.

3. Experimental Observations

The apparent lattice expansion in single crystal aggregates amounts to about 2.5 % for particles consisting of some 25 atoms, and it increases to as much as 7 % if the aggregates consist of only 6 atoms. Lattice expansions of this magnitude for particles in this size range were recently demonstrated in our laboratory for the case of palladium aggregates epitaxially grown on MgO (7). Particle deposition and subsequent TED and TEM examination were performed in-situ under 10^{-8} mbar vacuum conditions to exclude major influences by residual gases. The present work suggests that this observation may at least in part be explained as a diffraction phenomenon rather than an actual increase of the interatomic distances in the aggregates.

On the other hand, similar in-situ TEM observations for palladium on mica (8) yielded positive evidence for lattice expansion. In this case, the expansion for 1.5 nm particles, when compared to 5 nm particles, was measured to be $(2.8 \pm 0.3)\%$. The particles not being epitaxially oriented, our calculations (Fig. 6) predict only a very small apparent lattice parameter change for particles in this size range, and the observed lattice expansion must, therefore, be assumed real.

CONCLUSIONS:

Scattering patterns of very small metal aggregates have been calculated earlier, and some of the conclusions drawn from the present work have been formulated in the past. However, in view of the recent increase in interest in very small particles, spurred by catalysis research and the concommitant development of TEM diffraction studies on nanometer-size aggregates, it is worthwhile to recall some of the important points which are often neglected. The Scherrer- broadening effect suggests that the scattering patterns should always be divided by the rapidly decreasing function f_A^2 before any attempt is made to derive a lattice parameter from the reflection maxima. In the case of epitaxially oriented aggregates, this procedure effectively corrects for the low-angle displacement of peak maxima from which one otherwise might erroneously deduce a lattice expansion. However, in the case of aggregates in fully random or azimuthally random ('textured') orientation, the reflections are not resolved into discrete Debye-Scherrer rings if the aggregates consist of fewer than about 200 atoms. Therefore, the lattice parameter cannot be derived from a conventional analysis of the scattering pattern, not even after dividing by f_A^2. The only way to derive an accurate unit cell parameter is then to Fourier transform the scattered intensities to get a radial distribution of the atoms, indicating the exact interatomic distances.

The calculation of scattering patterns of model particles can

also be useful for analyzing the morphology of strongly anisotropic aggregates. For example, due to their different scattering patterns, very flat aggregates ("rafts") consisting of only a few atom layers can in principle be distinguished from spherical aggregates.

Acknowledgements

This work was supported by NASA under Grant No. NCC 2-283. We also gratefully acknowledge financial support by Alcoa Foundation to Eloret Institute for this work.

REFERENCES:

---

(1) L.H. Germer and A.H. White, Phys. Rev. 60 (1941) 447.

(2) C.R. Berry, Phys. Rev. 88 (1952) 596.

(3) G.W.B. Grigson and E. Barton, Brit. J. Appl. Phys., 18 (1967) 175.

(4) B.F. Warren, "X-Ray Diffraction," Addison-Wesley, Menlo Park, 1969, p. 116.

(5) J.M. Cowley, Diffraction Physics, North Holland Publ. Co., New York, 1981.

(6) D.J.C. Yates, L.L. Murrel, and E.B. Pestridge, J. Amer. Chem. Soc. 89 (1967) 4792.

(7) K. Heinemann, T. Osaka, H. Poppa, and M. Avalos-Borja, J. Catalysis 83 (1983) 61.

(8) K. Heinemann, submitted for publication.

(9) H. Poppa, R.D. Moorhead, and K. Heinemann, submitted for publication.

TABLE I

Apparent Change of Lattice Parameter (%)

Particle Diameter	No. of Atoms per Particle	111 **	200 ***	<101> texture ****	Fully Random Particle orientation ****
0.7	6	7.03	6.23	6.70	8.80
0.8	13	3.79	3.33	1.06	0.97
1.4	55	1.29	1.17	-0.21	-0.15
1.6	87	0.97	0.86	0.24	0.28
2.0	188	0.50	0.42	0.61	0.80
2.6	490	0.33	0.27	0.38	0.39
3.7	1464	0.15	0.15	0.23	0.23

* Spherical particle models, all atoms in bulk positions.

** Single particle diffraction, particle in <101> orientation, and 111 reflection evaluated.

*** Single particle diffraction, particle in <101> orientation, and 200 reflection evaluated.

**** Multiple-particle diffraction, 111 diffraction ring evaluated.

TABLE II

Intensity Ratio Between First and Second (311 when resolved) Peaks

No. of Atoms per Particle	Particle Orientation:	
	azimuthally random	fully random
6	3.90	3.32
13	4.38	3.89
55	4.46	3.82
135	4.70	3.64
976	8.84	4.11

FIGURE CAPTIONS

Fig. 1(a) Atomic Scattering profile f_A^2 (squares) and interference function (circles) in <100> direction as a function of $\sin\frac{\theta}{\lambda}$ for a 13-atom Pd model in <100> orientation (atoms in the bulk positions; peaks are at bulk positions).

(b) Total electron scattered intensity as a function of $\sin\frac{\theta}{\lambda}$ for the model of Fig. 1a. Note the change in peak position, representing an apparent lattice expansion.

Fig. 2 3-D schematic representation of 90-sectors in the diffraction plane for various particle models. The vertical axis is proportional to the intensity. The atoms are placed in the bulk positions (<100> zone axis).

Fig. 3 Apparent lattice expansion, calculated by comparing computed diffraction peak positons of clusters with those of bulk material, as a function of the size of the clusters, for epitaxial, <100> - oriented aggregates.

Fig. 4 3-D schematic representation of 90° sectors in the diffraction plane for various particle

models. The vertical axis is proportional to the intensity. The atoms within each cluster are placed in the bulk positions. The clusters are in random orientation with respect to each other.

Fig. 5 Diffraction profiles computed for spherical cluster models of various sizes in random orientation.

Fig. 6 Apparent change in lattice parameter (calculated as for Fig. 3) as a function of particle size, for fully randomly oriented particles (dash-dot curve) and for (<101>) textured particles in random azimuthal orientation (dash curve).

Fig. 7 Diffraction profile for an infinite number of particles in random orientation, each composed of two (100) layers with a total of 81 atoms (a), and of two (111) layers with a total of 90 atoms (b).

Fig. 8 Diffraction profiles computed for particles with 2.4 nm projected size in random orientation: a) clusters with an overall spherical morphology; b) rafts made of three (111) layers.

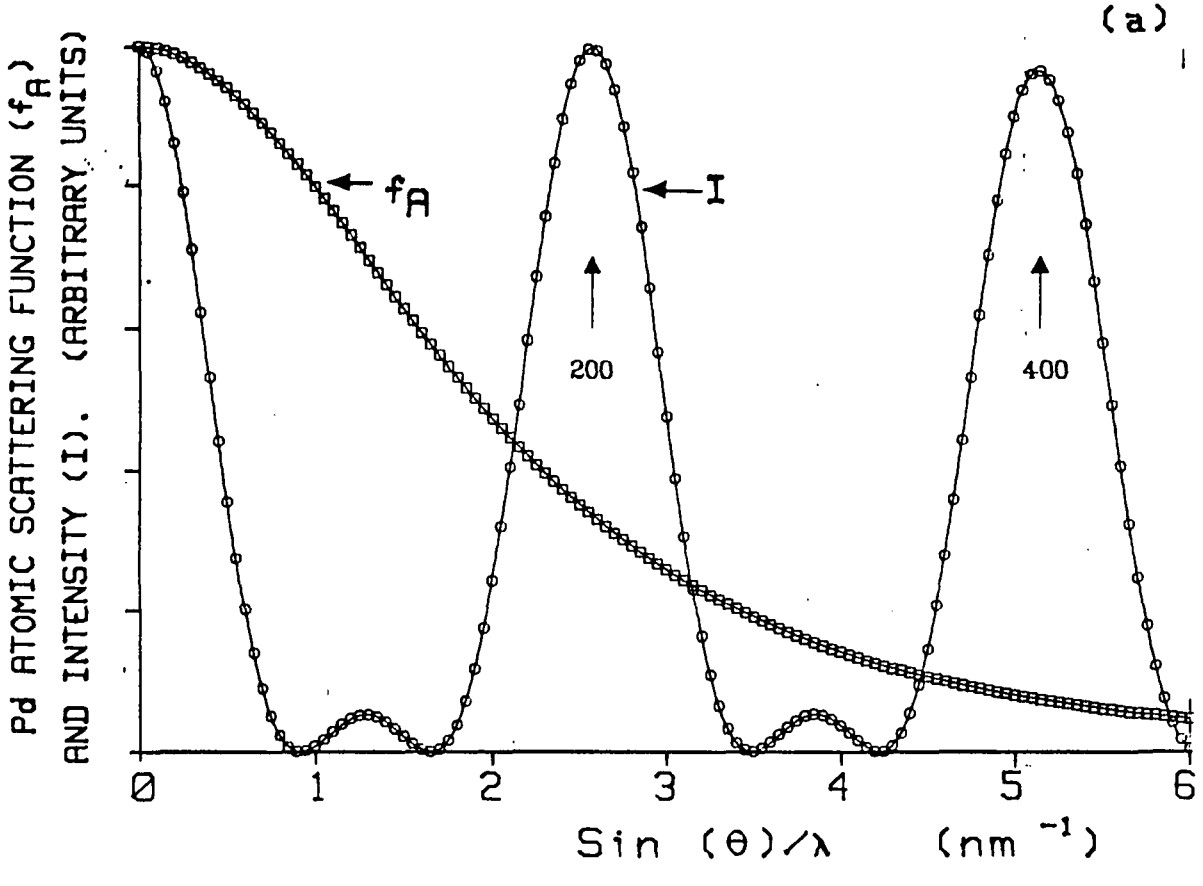
(a)
Pd ATOMIC SCATTERING FUNCTION (f_A)
AND INTENSITY (I). (ARBITRARY UNITS)
f_A
I
200
400
0
1
2
3
4
5
6
Sin (θ)/λ (nm $^{-1}$)

Fig. 1a

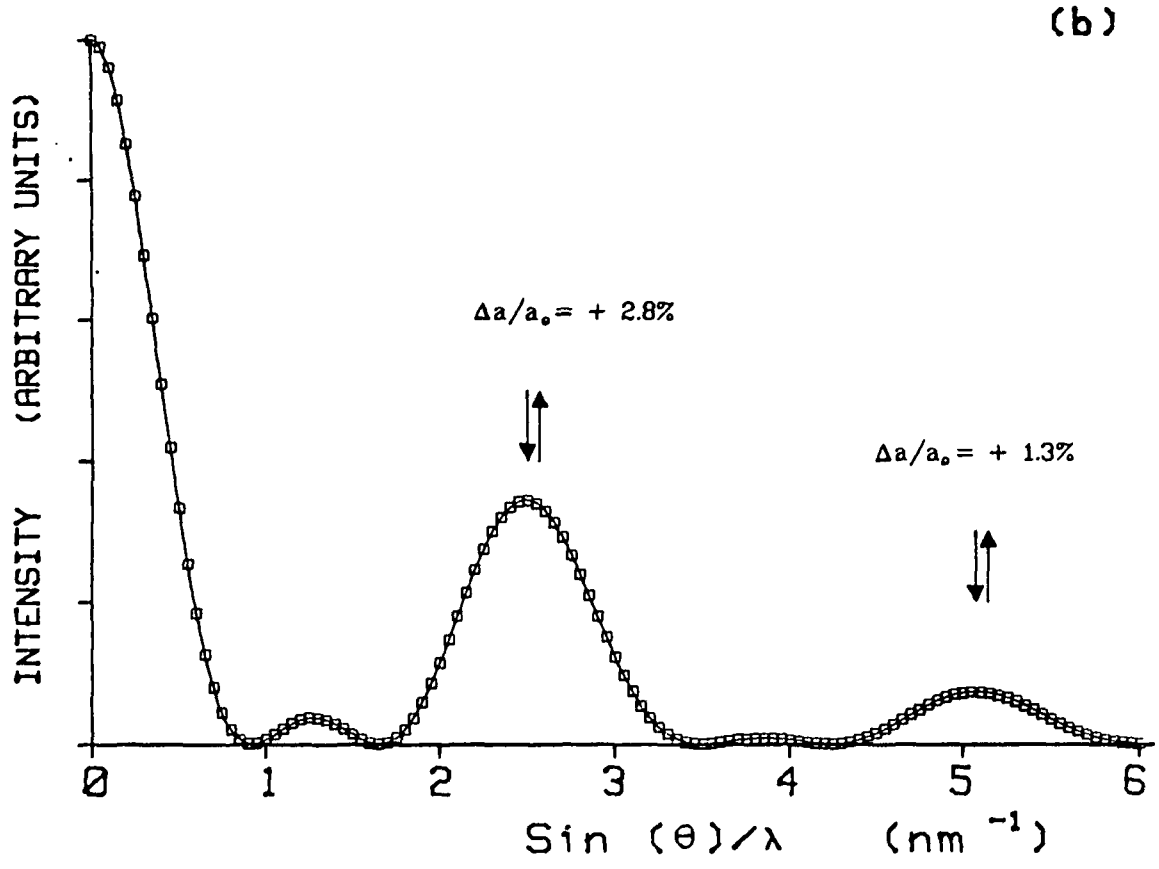
(b)
INTENSITY (ARBITRARY UNITS)
Δa/a₀ = + 2.8%
Δa/a₀ = + 1.3%
0
1
2
3
4
5
6
Sin (θ)/λ (nm⁻¹)

Fig. 1b

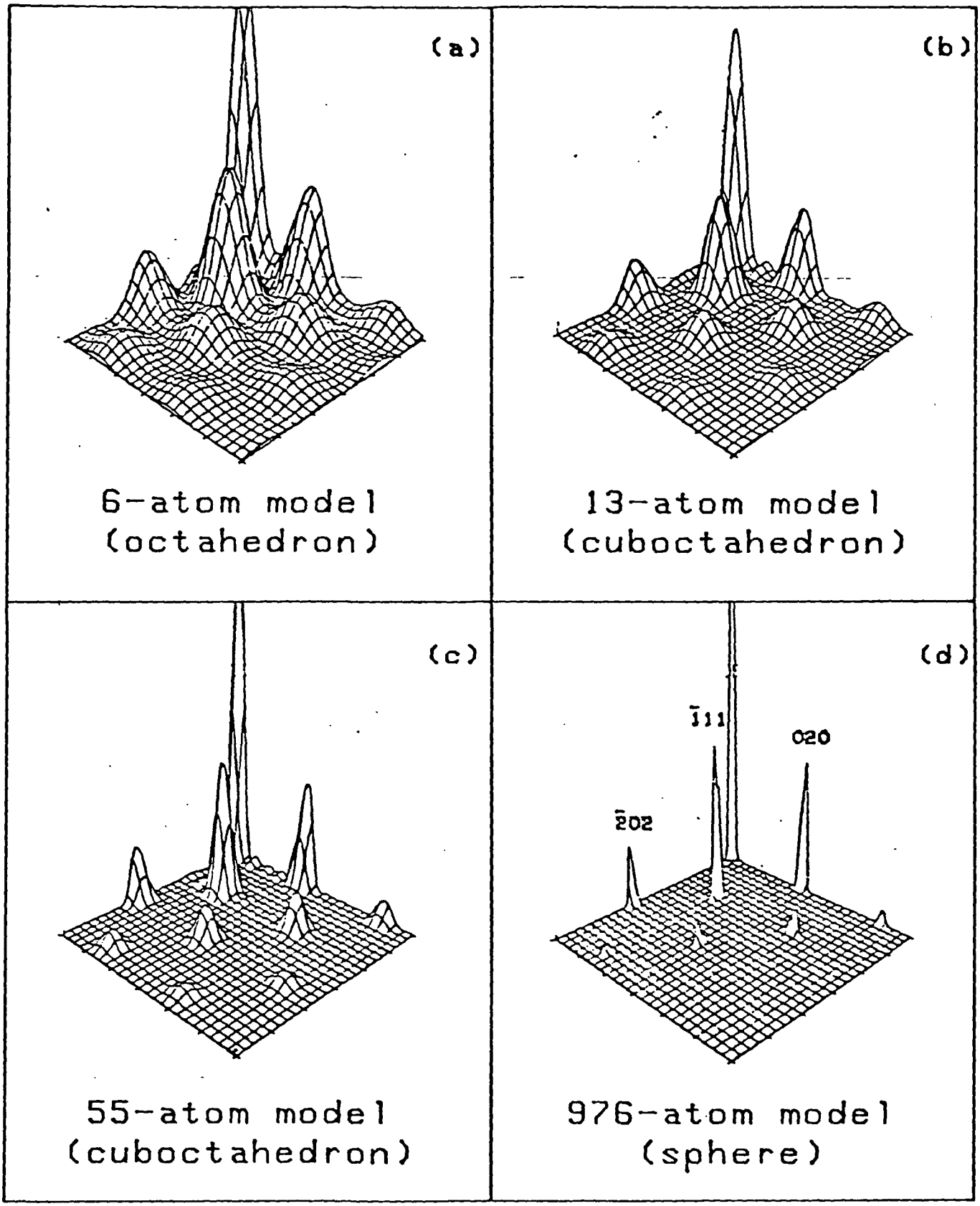
(a)
6-atom model
(octahedron)
(b)
13-atom model
(cuboctahedron)
(c)
55-atom model
(cuboctahedron)
(d)
$\bar{1}11$
020
$\bar{2}02$
976-atom model
(sphere)

Fig. 2

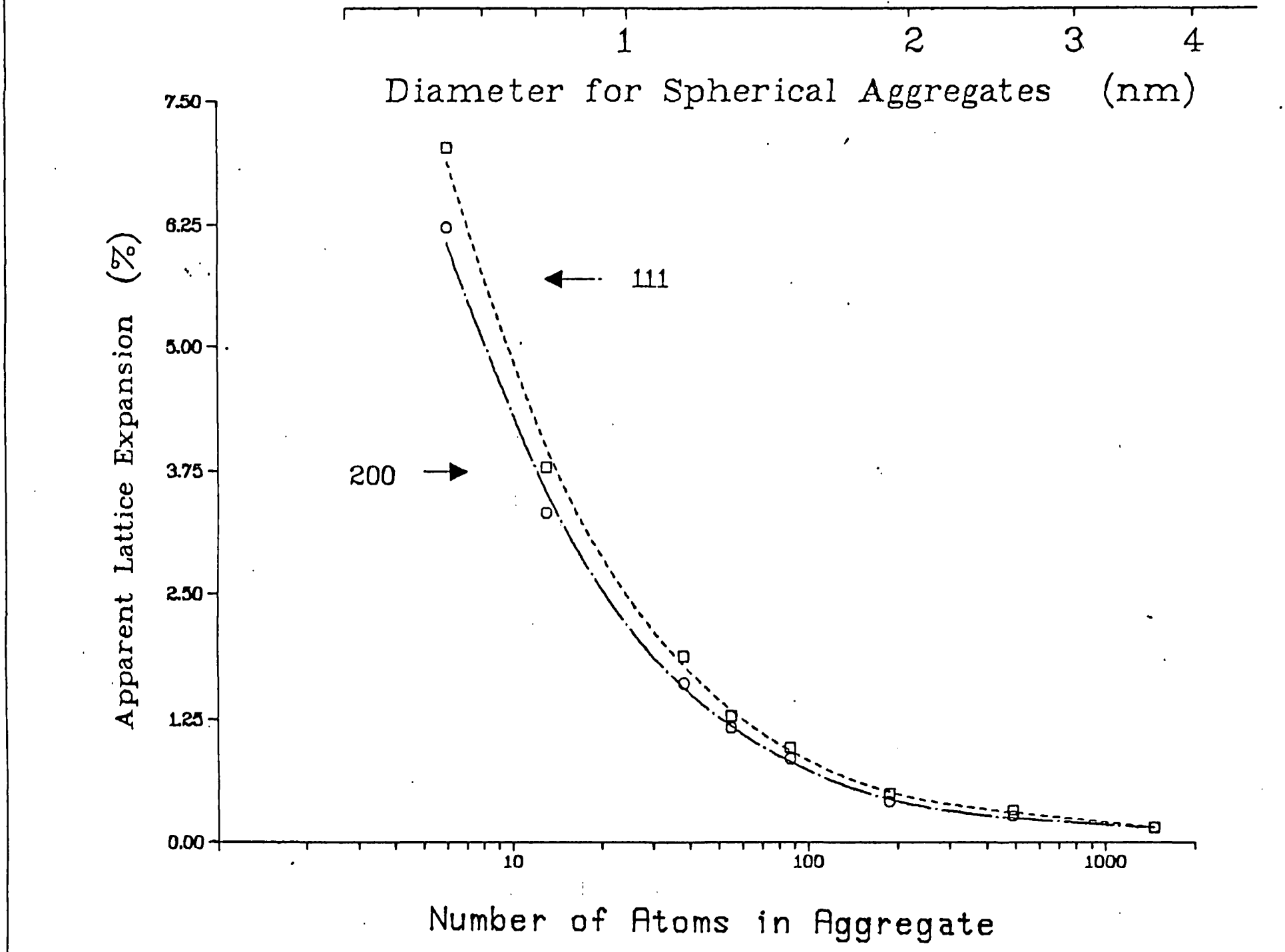
1
2
3
4
Diameter for Spherical Aggregates (nm)
7.50
6.25
5.00
3.75
2.50
1.25
0.00
Apparent Lattice Expansion (%)
111
200
10
100
1000
Number of Atoms in Aggregate

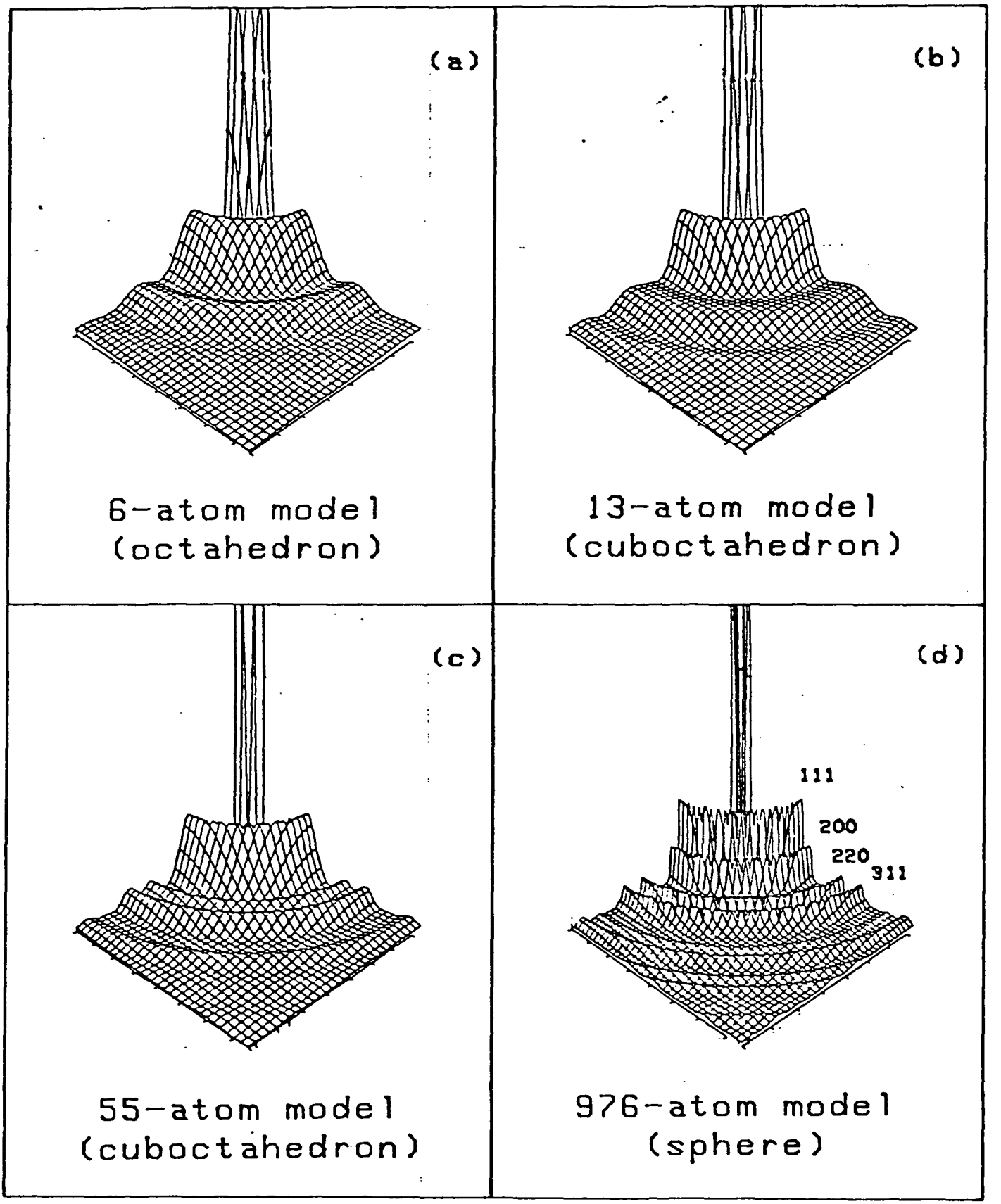
(a)
6-atom model
(octahedron)
(b)
13-atom model
(cuboctahedron)
(c)
55-atom model
(cuboctahedron)
(d)
111
200
220
311
976-atom model
(sphere)

Fig. 4

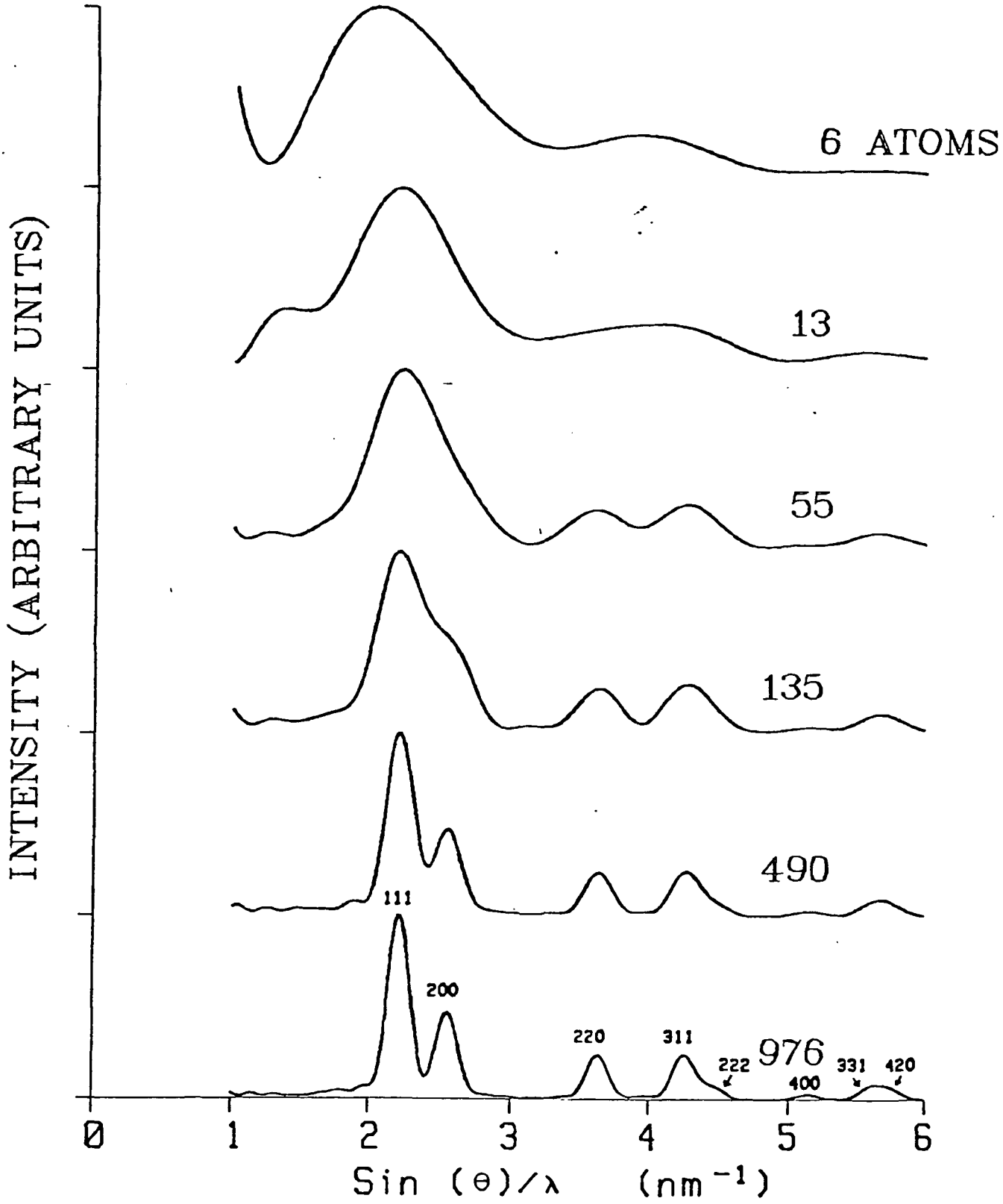
6 ATOMS
13
55
135
490
976
111
200
220
311
222
400
331
420
INTENSITY (ARBITRARY UNITS)
0
1
2
3
4
5
6
Sin (θ)/λ (nm⁻¹)

Fig. 5

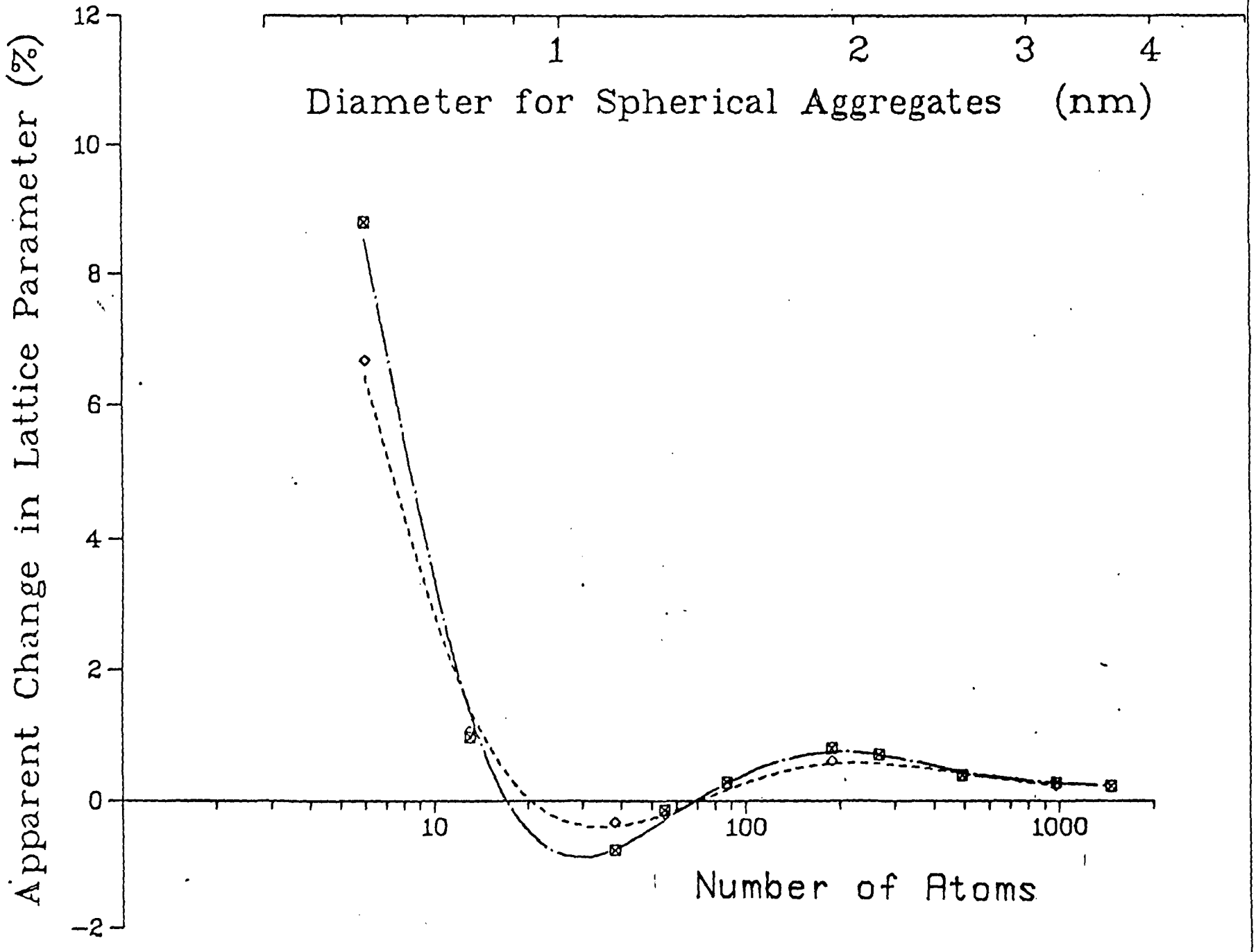
Apparent Change in Lattice Parameter (%)
12
10
8
6
4
2
0
-2
1
2
3
4
Diameter for Spherical Aggregates (nm)
10
100
1000
Number of Atoms

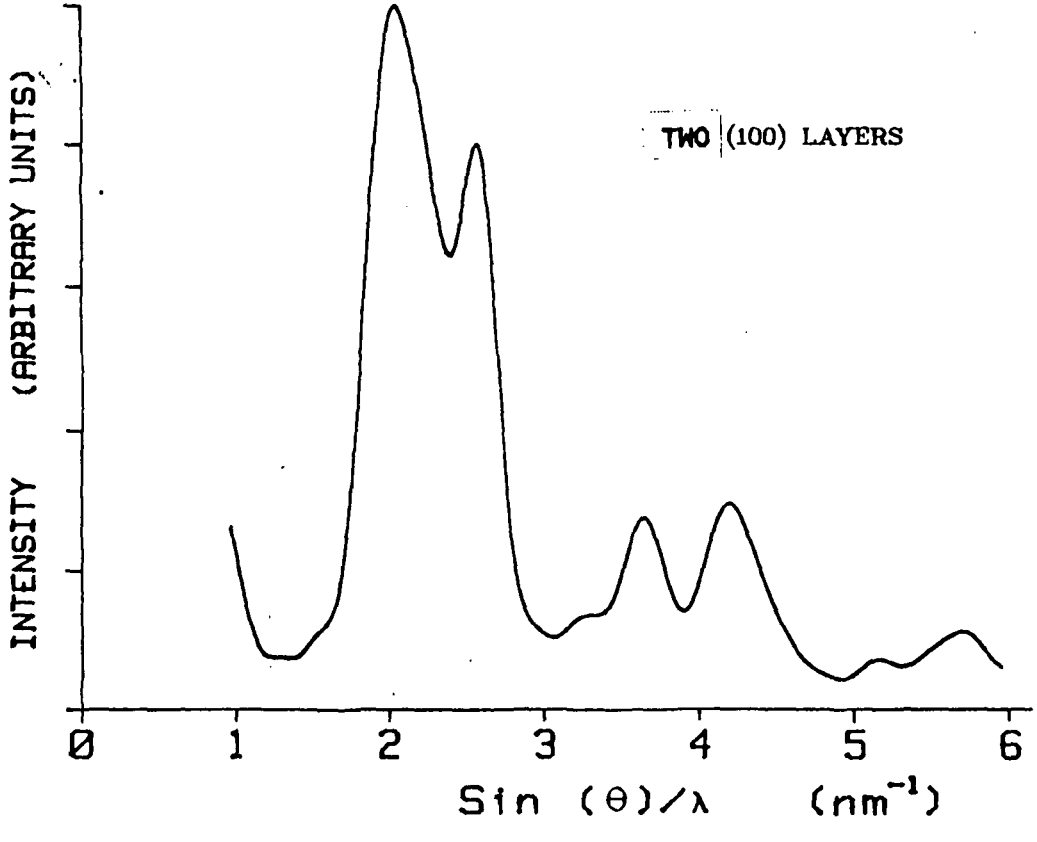
TWO (100) LAYERS
INTENSITY (ARBITRARY UNITS)
0
1
2
3
4
5
6
Sin (θ)/λ (nm^{-1})

Fig. 7a

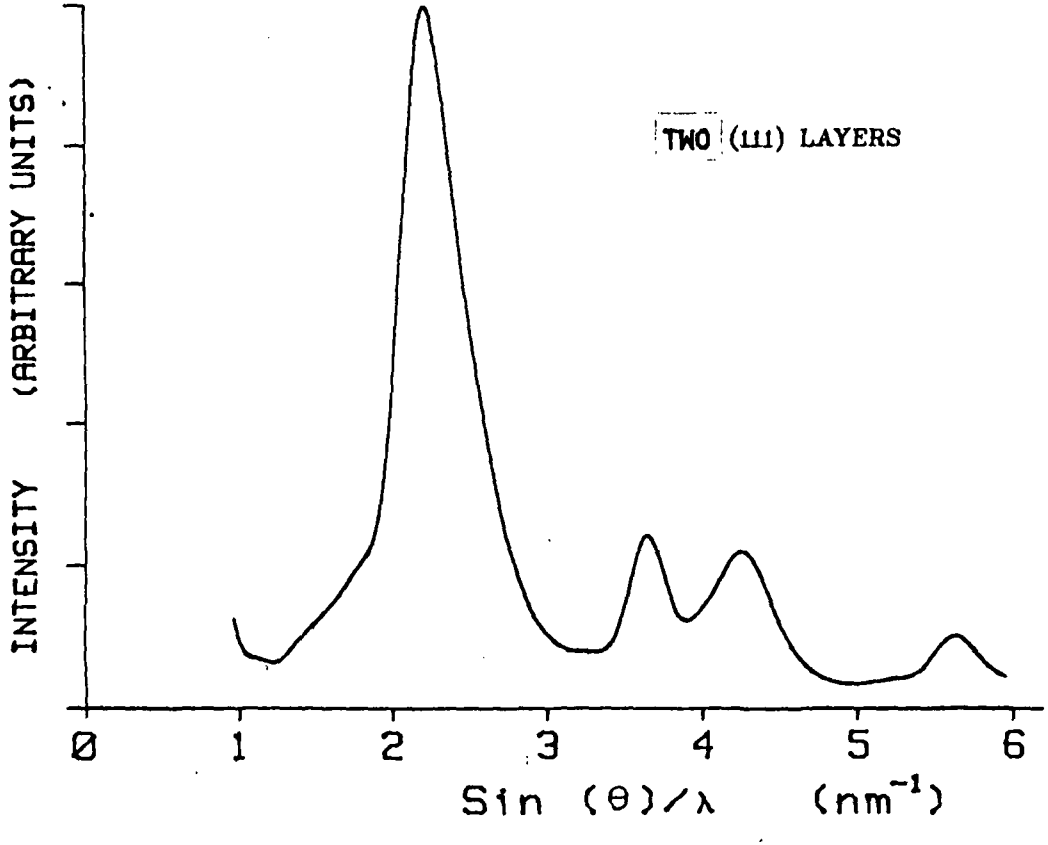
TWO (111) LAYERS
INTENSITY (ARBITRARY UNITS)
0
1
2
3
4
5
6
Sin (θ)/λ (nm⁻¹)

Fig. 7b

(a)

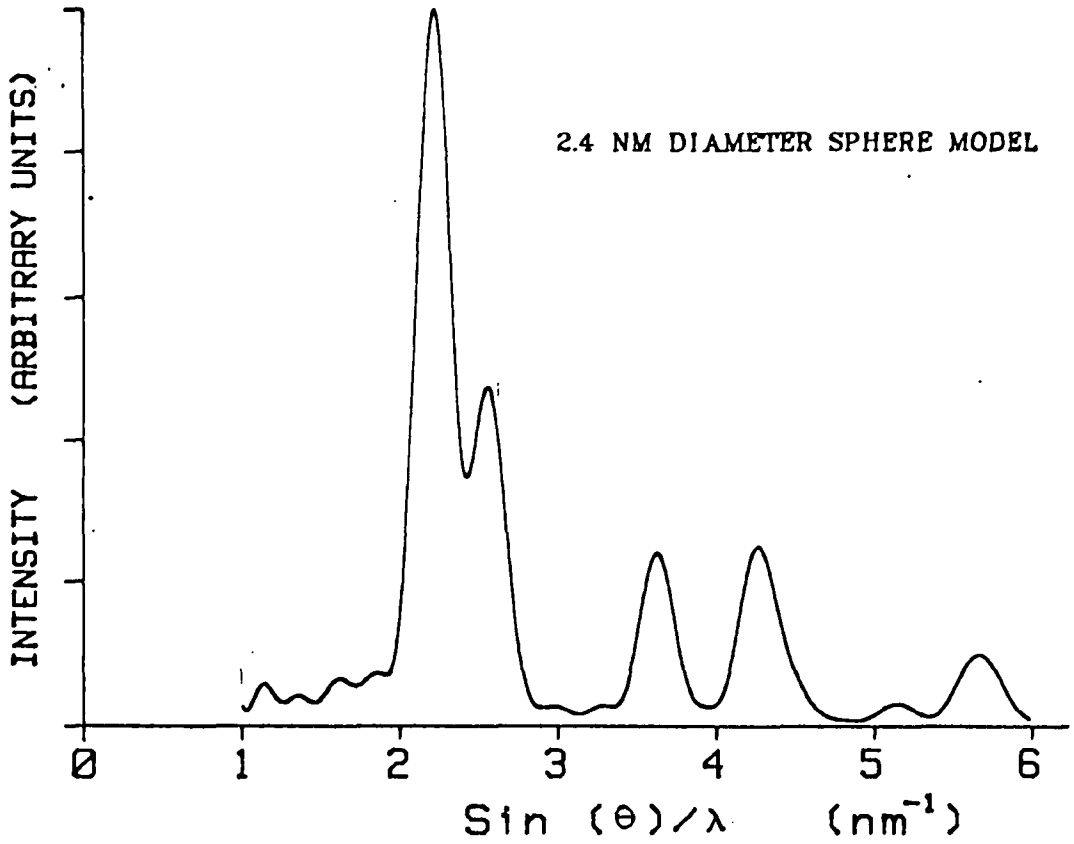
2.4 NM DIAMETER SPHERE MODEL
INTENSITY (ARBITRARY UNITS)
0
1
2
3
4
5
6
Sin (θ)/λ (nm⁻¹)

Fig. 8a

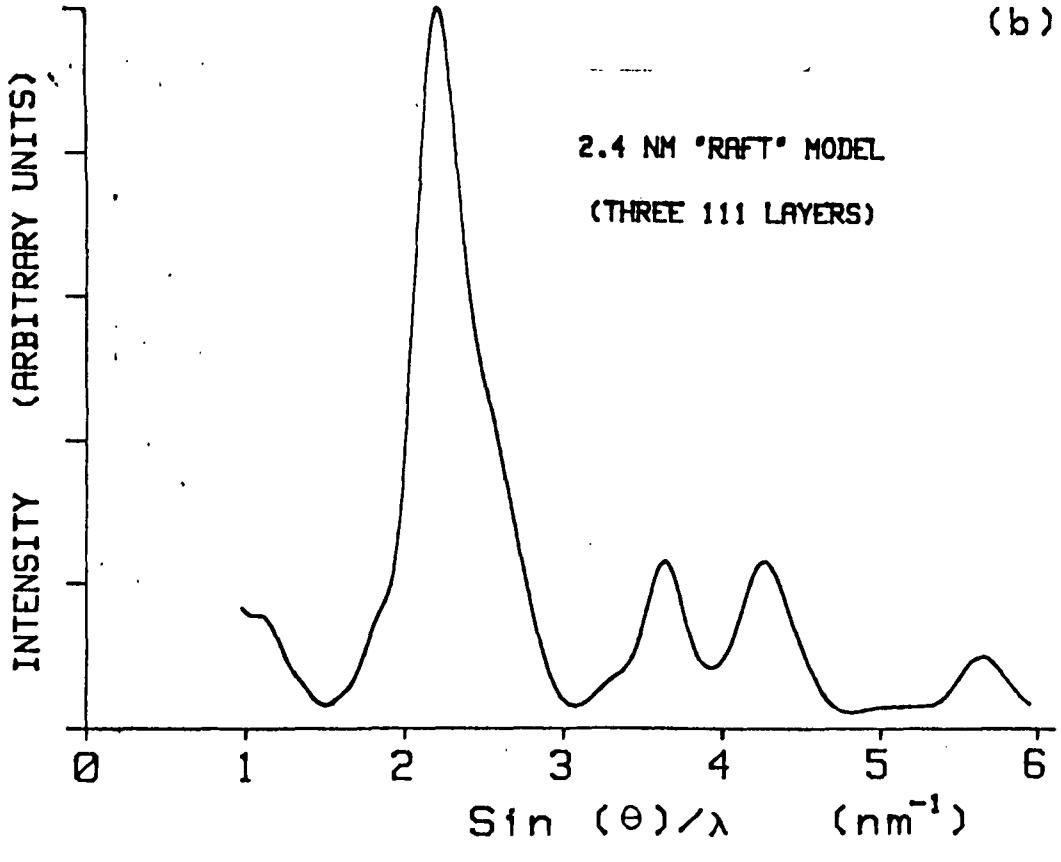
(b)
2.4 NM "RAFT" MODEL
(THREE 111 LAYERS)
INTENSITY (ARBITRARY UNITS)
0
1
2
3
4
5
6
Sin (θ)/λ (nm⁻¹)

Fig. 8b

APPENDIX 3

Preparation and Analysis of Particulate Metal Deposits

by

H. Poppa, D. Moorhead, and K. Heinemann

Stanford/NASA Joint Institute for Surface &

Microstructure Research

Moffett Field/CA 94035

Chapter 1

Summary

Small particles and clusters of Pd were grown by deposition from the vapor phase under UHV conditions. Amorphous and crystalline support films of alumina and ultra-thin amorphous carbon films were used as substrate materials. The growth of the metal deposit was monitored in-situ by scanning transmission diffraction of energy-filtered 100 KV electrons and high-resolution transmission electron microscopy (TEM) analysis was performed in a separate instrument. It was etsablished by in-situ TEM, however, that the transfer of specimens in this case did not unduly affect the size and distribution of deposit particles. It was found that the cleanliness, stoicheometry, crystallinity, and structural perfection of the support surface play an essential role in determining the crystalline perfection and structure of the particles. The smallest Pd clusters reproducibly prepared contained not more than 6 atoms but size determinations below 1 nm average particle diameter are very problematic with conventional TEM. Pd particles grown on carbon supports feature an impurity stabilized mosaic structure.

Chapter 2

Introduction

The advent of advanced UHV technologies and sophisticated techniques of surface analysis has renewed interest in studies with very small supported metal particles and clusters. However,only very limited experimental work of a systematic nature can be found regarding the well-controlled preparation and analysis of particles less than 2 - 3 nm in size [1]. This is unfortunate because particles in that size range and smaller are of prime interest in many promising areas of application in model catalysis,optics,and thin film electronics [2].

The microscopic structure of supported particles and clusters containing from 10 to 1000 atoms is difficult to discern by high resolution transmission electron microscopy (TEM), mainly because of imaging interference by the supporting material and because of diminishing image contrast. It becomes imperative,therefore,to choose suitable thin film supports both for TEM of individual,nanometer-size particles and for transmission electron diffraction (TED) studies where the contributions of many similar particles are integrated. Furthermore,if the microscopic

analysis of very fine particulate deposits is to be meaningful and useful for the measurement of surface properties, the preparation of the ultra-thin deposit and its microscopic analysis have to be performed in one UHV environment, unless it has been verified that exposure to air during transfer from the (UHV) deposition and analysis system to the electron microscope or diffraction instrument has negligible influence on the particle structure. Only when negligible influence has been demonstrated is it reasonable to combine UHV deposition and surface analysis of the metal particles with standard high resolution microscopy and diffraction analysis in an integrated experimental approach [3]. It then becomes possible to correlate the size and microstructure of vapor deposited metal particles with their physical, chemical, and electronic properties in a reliable manner [3].

In this report, we are concentrating mainly on the crystallographic properties of clean particles and clusters.To our knowledge, there is no definite information available at the present time that would correlate particle size and (long-range) crystallographic order. The remaining most elusive particle property is the particle morphology or shape , which will probably have to be inferred indirectly by comparison with cluster calculations [4] and gas adsorption/reaction rate measurements [3], [5].

Chapter 3

Experimental

Previously used versions of UHV in-situ TEM and STED (Scanning Transmission Electron Diffraction) instruments [2] have been upgraded with the addition of sample introduction (SI) facilities. Fig. 1 shows a schematic rendering of the combined TEM/STED system with wire-source evaporator and SI device in the differentially pumped UHV specimen chamber and with image intensifier and spectrometer facilities (for energy filtering of diffracted electrons) as detectors.

The background pressure level for the present experiments was in the 1 - 2 x 10(-9) mbar range due to the superior outgassing characteristics of low-mass wire sources. CO, H2, H2O, and CO2 are dominating the residual gas spectrum.

The newly developed sample introduction device was instrumental for the success of the present series of experiments, because it permitted not only the rapid exchange of test specimens without the need for repeated baking cycles , but also because cleaning treatments of the surface of the supporting film prepared outside the in-situ instrument became routine, and because metal deposits

could be easily oxidized and reduced at room temperature. The latter was accomplished by exposing the sample surface to an rf oxygen (or hydrogen) plasma discharge at room temperature inside the sample introduction chamber; the sample was thereby exposed to highly activated atomic and molecular gas species. Each sample used in this study was routinely cleaned before introduction into the UHV chamber by exposure to an oxygen plasma which lasted a few seconds for ultra-thin carbon supports and several tens of seconds for alumina films. The cleaning effect that this treatment has on the surface composition of an anodic Al2O3 film is shown in the Auger spectrum of fig. 2.

The high resolutiom TEM micrographs produced in the course of this study were obtained with a standard high resolution instrument in order to assure the highest possible image quality for very small metal particles. As pointed out earlier, this is permissible only for a combination of support and deposit materials that has been proven not to be affected appreciably by room temperature exposure to laboratory air and subsequent exposure to the imaging electron beam. The in-situ TEM images of the same specimen area of a beam recrystallized alpha-Al2O3 (α-Al_2O_3) support region with room temperature deposited Pd particles before and after air exposure show (fig. 3) that both particle number densities and average particle sizes are not affected in this case. This micrograph represents the limit of resolution of our in-situ TEM and it is ,therefore, impossible to make any

statements concerning changes in particle shapes; but some small particle translations were definitely observed. This result is in contrast to the much more marked changes upon air exposure that were previously found for Pd particles deposited on beam-cleaved MgO supports [6].

Dealing with the problem of background interference from support is absolutely essential for the success of small particle studies in both high resolution imaging [7] and in high sensitivity STED [2, 3] . For the present model studies, we have reduced the support background in two ways using ultra-thin carbon prepared by 'shadow evaporation' onto mica [8] and anodically oxidized amorphous alumina films that can be e-beam recrystallized in-situ [9] . How these two thin film supports compare with other support materials in terms of background diffraction intensities is demonstrated in fig. 4 . It is clear that for the case of metal deposits that have strong diffraction intensities at 1/d values similar to Pd, recrystallized -alumina and ultra-thin carbon are by far the best choices.(Of course, alumina grains of suitable orientation have to be selected. For Pd this usually means no appreciable alumina diffraction intensity around 1/d = .445 and possibly .727) .

Amorphous alumina films of appropriate thickness can be easily recrystallized in-situ with a high intensity e-beam. Fig.5 shows a micrograph and the corresponding transmission diffraction pattern of such a film. Fears that this kind of high temperature

treatment might affect the alumina surface composition have been alleviated by the possibility of oxygen saturation of this surface by exposure to an oxygen plasma in the SI chamber before metal deposition.

Low evaporation rate 'dosage sources' have been used for metal deposition. They have been popular in surface science studies of metal deposits on metallic substrates for many years (e.g., [10]) and have proven to deliver stable low dosages of metal evaporants over long periods of time. Such a source, consisting of fine Pd wire wound around a thick stranded coil of W wire, is resistance heated by a constant current, which results in the source temperature characteristics depicted in fig. 6. After an induction period of about 35 seconds, the source temperature has reached about 90 % of its final temperature at 3 min of operation. The amount of Pd delivered was estimated from the size and number density of Pd particles resulting from 3 min depositions onto C substrates at room temperature (RT) assuming hemisperical particle shapes and unity sticking coefficient . An average metal thickness of approximately .125 nm was calculated, which corresponds to about .83 monolayers(ml) of Pd for each 3 min deposition. For the alumina substrates, a three times lower sticking coefficient was found resulting in a dosage of approximately .10 nm of Pd (or .65 ml) for a 6 min deposition.(This trend of a higher sticking coefficient on C agrees with the observations for all other metals except Pd(!) in

[1]).Since a 1x3 min deposition on C and a 1x6 min deposition on Al2O3 resulted in Pd particles that were just barely distiguishable by high-resolution TEM, we chose deposition times of 3 and 6 min increments as standards in this study.

The recognition of metal particles of less than about 1 nm in size is a difficult TEM problem as was noted before. The approach we have taken is discussed in conjunction with fig.7 which shows two defocus settings of high magnification micrographs of a 3 min deposit on C. The phase contrast background structures of the amorphous support interfere strongly with particle recognition. In counting particles of this small size we have generally adopted the position that a particle is registered only if it is recognized on two micrographs taken with either two differing defocus settings or with two different small objective lens apertures (in both cases the background structures change drastically). The determination of actual particle sizes is,of course,even more controversial for ultra-thin deposits Extreme care must be taken ford sizes below 1 nm where imaging very near the Gaussian focus and total correction of astigmatism are an absolute requirement. We generally take the rigorous position that a size determination with an accuracy better than +—0.2 nm is not possible by conventional high-resolution TEM.

A significant improvement in particle recognizability derives from the use of single crystal support films as opposed to amorphous ones .This is demonstrated with fig.8 which compares

(2x6 min) depositions on amorphous alumina (a-Al2O3) and on beam recrystallized α-Al2O3. Obviously there is much less structural background interference in the single crystal support case, which has been noted previously [11], [12], [13] and single crystal supports were used with great advantage during catalytic oxidation studies of CO over very small Pd particles supported on sapphire [14], as well as during gas exposure studies of very small Pd particles supported on MgO [15], [6].

Chapter 4

Results and Discussion

4.1 RT Growth of Pd on Carbon and Alumina

The 4 depositions of Pd on C shown in fig. 9 are used to demonstrate that dosage sources are useful for varying the size of the deposited particles with reasonable control. It is important to notice the constant number density of particles which indicates that the nucleation phase for these RT depositions of high supersaturation is already completed after the first 3 min of deposition and the maximum number density of particles has been reached. Subsequent depositions only increase the particle size with a growth rate averaging about 2 atoms per min per particle (not reliably established at present). It seems clear,however,that the growth rate increases with particle size which could suggest growth occuring primarily by direct impingement.

The scanning diffraction intensities recorded in-situ immediately following each Pd deposition, and corresponding directly to the TEM results of fig. 9, are displayed in fig. 10. Similar STED data, but for the deposition of Pd on amorphous and beam recrystallized single crystal regions of an Al2O3 support film, are shown in fig.11a and 11b, respectively. It is clear that the highest sensitivity for detecting particulate metal films by transmission electron diffraction (TED) is achieved on α-Al2O3 with the lowest and smoothest diffraction intensity in the 1/d region of the combined (111)+(200) Pd peak. From other diffraction data it was determined that the conservative limit of detection by energy-filtered STED is around 1/3 of a single Pd dosage, i.e. at about 1/5 of an average monolayer (ml) deposit. Such ultra-thin deposits, consisting of particles of certainly no more than 6 atoms, are extremely difficult to analyze by conventional TEM methods and high-sensitivity STED may be more useful.

Average particle sizes and (maximum)number densities are listed in table 1 where a distinction is made between particle diameters directly measured from micrographs D(TEM) and particle sizes deduced from broadening measurements of diffraction intensities D(STED) (Debey-Scherrer broadening, see later). In general, the Pd particles on C tend to be somewhat smaller and their number densities higher than on Al2O3. This tendency could be in part responsible for the much poorer resolution of the (200) Pd peak

in all deposits on C. However, there are small particle deposits (2x6 min) on oxygen treated Al_2O_3 (Al_2O_3+) that show a reasonably well resolved (200) peak and even large particle deposits on C (4x3 min) do not exhibit a resolved (200) peak. At the same time, the (220) and (311) peaks of the 4x3 min deposit in fig. 9 are clearly visible . The latter fact could be explained by a (211) growth texture, but this is very unlikely and another interpretation of this result may be more appropriate: The larger Pd particles grown on C at RT and even more so at elevated temperature are probably composed of a mosaic of small single crystal blocks no more than about 1.0 - 1.7 (for the high-T deposits) nm in size. This interpretation is supported by the form of diffraction intensity profiles calculated from perfect f.c.c. clusters [16]. The profile of a 55 atom cluster is very similar to the 4x3 min trace in our fig. 10 . One is, therefore, forced to conclude that this kind of disorder persists during the growth of Pd particles on C, and this type of growth causing a persistent 'line broadening' can be due to surface impurities originating either in the gaseous environment (our background pressure is of the order of 10(-9) mbar) or stemming from the carbon substrate. It is also interesting to note that these Pd deposits on C are quite stable during annealing. Temperatures above 500 C are needed to cause massive recrystallization of the particles.

The strong influence of support surface crystallinity and

composition can be directly assessed for the case of alumina supports where simultaneous deposition onto amorphous, recrystallized, and recrystallized and oxygen-plasma-treated support areas are possible (see fig.12). The particle sizes for oxygen treated α-Al2O3 surfaces in fig.12b and 12c are definitely larger than for only beam recrystallized α-Al2O3 in fig.12a and the 2x6 min deposits on oxygen treated α-Al2O3 are always showing a better resolved (200) Pd peak and improved geometrical particle shapes (i.e. improved crystallinity). These results are interpreted at present as due to a higher sticking coefficient of Pd on only beam-recrystallized α-Al2O3 and improved crystalline perfection and stoicheometry on the oxygen treated α-Al2O3 surface due to a diminishing influence of surface imperfections on metal nucleation and growth on this surface.

4.2 The Influence of Elevated Support Temperature on Growth

Although the bulk of the results obtained with metal deposits prepared and/or treated at elevated support temperatures will be published in the future, some of these findings have to be discussed in relation to RT depositions.

The TEM results of fig. 12 are complemented by the diffraction line profiles of fig. 13, which in addition provide information

on the influence of elevated support temperature on particle growth (all traces refer to 2x6 min deposits except 13f which corresponds to two 6 min plus one 8 min deposit). Extented annealing of RT deposits causes particle growth by ripening and coalescence and a corresponding sharpening of diffraction peaks (13c) and in addition to that a peak shift of about 2 % is observed indicating an increase in lattice spacing for the deposits made at an elevated support temperature of 180 C (13e and 13f). This lattice expansion of the deposit particles is probably due to epitaxial lattice matching (the corresponding diffraction patterns show strong epitaxial textures), is similar to the lattice expansion found for RT growth of Pd on clean MgO surfaces [6], and is contrary to the lattice contraction found for very small zeolite supported metal particles [17]. The dash trace in fig. 13 shows for comparison and contrast one results for amorphous Al2O3 which has been verified repeatedly: the (200) peak is very poorly accentuated indicating a somewhat higher degree of disorder than for comparable deposits on single crystal supports.

The most notable effects of elevated support temperatures in the context of this study in which low-rate dosage sources for metal deposition are routinely employed are the increase in particle size and the concomitant decrease in particle number density which are graphically represented in fig.14. The relatively narrow character of the size distribution at RT with a

FWHM of about 1 nm is lost by both annealing and high temperature deposition. So the gain in particle crystallinity, expected from elevated temperature experiments because of increased mobility on the support surface, is counteracted by this loss of particle size and size definition. However, this may be a peculiar feature of low-rate source arrangements and one is in general well adviced to utilize higher-rate metal sources in combination with short evaporation times and elevated support temperatures for an improved degree of long-range crystallographic order in vapor deposited small metal particles. Previous work with mica or sapphire supports proves that Pd and Ni particles well below 2 nm in size can be obtained [5,14], [18].

4.3 Diffraction Line Broadening

The question of long-range crystallographic order in vapor deposited particulate metal films is of considerable importance with respect to the usefulness of such deposits as catalytic model systems. Since comprehensive radial distribution function (RDF) calculations of our STED results are not yet available , it was attempted to analyze the diffraction results in terms of simple Debey-Scherrer line broadening . Specifically , we tried to fit the combined diffraction line profiles of the as-measured Pd (111) + (200) peak with two separate Gaussian line profiles corresponding to the (111)and the (200) peak,respectively. The

peak widths at half maximum of the two Gaussian peak components that reproduced the experimentally recorded peak profiles best were then interpreted with the well-known line broadening formula [19] adapted for the case of high energy transmission electron diffraction (see for instance [20])

$$D_{STED} = \left\{ \frac{\Delta R - a}{R} \times \frac{1}{d} \right\}^{-1}$$

where R and ΔR refer to the radius and width of the experimentally measured diffraction line, respectively, and where 'a' is the instrumental line width (in our case about 0. 169 nm(-1)). The curve fitting procedure is indicated in fig.15, in which case two Gaussians of 2 : 1.1 peak ratio with a peak width of .0225 (in 1/d units) were used. The broadening deduced average particle size is 2.4 nm, which compares very well with the TEM measured particle size of about 2.5 nm (for this 2x6 min deposit on oxygen treated α-Al2O3). It has to be concluded, therefore, that the line broadening is fully accounted for by the small size of the diffracting Pd particles and no additional crystalline disorder is indicated. Comparing the microscopy and diffraction determined particle diameters D(TEM) and D(STED) in table 1 shows clearly that for most of the Pd depositions on single crystal Al2O3 the particles seem well ordered. There is, however, a tendency towards less order for Pd particles deposited at RT onto a-Al2O3 (the particular case for particles on amorphous carbon was discussed in section 4.1). This conclusion has to be qualified, however, for very small particles because the average particle size D(TEM) measured for such

deposits could easily be misleading due to the inherent difficulties of obtaining meaningful size distributions .

Chapter 5

Conclusions

In-situ and ex-situ transmission electron diffraction and microscopy studies have been used to analyze the requirements for preparing well-ordered Pd particles and clusters by UHV vapor deposition on suitable supports. In particular it was established that

1) the crystallinity, cleanliness, stoicheometry, and structural perfection of the support surface play a major role in determining the crystalline perfection and structure of the supported particles. Since these support surface characteristics are influenced by the vacuum environment during deposition, it is also essential to work at the lowest possible background pressures. Background pressures of the order of 1 - 2x10(-9)mbar were found in this study to be sufficient for alumina supports but serious problems were indicated for the use of carbon substrates.

2) Pd particles grown on carbon supports at temperatures ranging from RT to about 550 K were found to have an impurity stabilized mosaic structure(with individual crystalline blocks of

about 1 - 1.5 nm). Annealing temperatures in excess of 800 K were required to cause recrystallization (and further particle growth). The impurity in question could be carbon from the support.

3) At 300 K deposition temperature, low-rate metal evaporation sources provide reasonable control of particle size. The smallest clusters reproducibly prepared contained not more than approximately 6 Pd atoms. However, size determinations by CTEM below 1 nm are very problematic. Deposits with an average particle size of 1.5 nm or larger can be easily produced featuring size distribution half widths of about 1 nm. Larger particles with wider size distributions resulted from deposition at elevated support temperatures or from annealing.

4) Thin single crystal support films are not only preferred because they promote particle crystallinity but also because they enhance the detection and analysis of very small supported particles and clusters.

Chapter 6

Figures

Fig. 1 : Schematic of UHV STED/TEM system with low rate evaporation source and sample introduction and treatment facility.

Fig. 2 : Auger spectrum of a-Al2O3 support film surface before and after oxygen plasma cleaning.

Fig. 3 : The same α-Al2O3 specimen area before Pd deposition (a), immediately following RT deposition of very small Pd particles (b), and after exposure to laboratory air (c).

Fig. 4 : Energy-filtered scanning transmission electron diffraction (STED) recordings of various thin film support materials.

Fig. 5 : TEM micrograph and TED pattern of e-beam recrystallized α-Al2O3 support film region.

Fig. 6 : Starting temperature characteristics of wire evaporation source.

Fig. 7 : 3 min deposition of Pd at RT on ultra-thin amorphous

Table

Average deposit parameters for Pd on alumina and carbon supports

T_s	$t_{deposit}$	Support	Particle #-Density	D_{TEM}	D_{STED}
300 K	1x6 min	α-Al2O3	7.5x10(+12) cm(-2)	0.9-1.4 nm	NA
300	1x6	α-Al2O3+	7.0	1.2-1.5	NA
300 K	2x6 min	α-Al2O3	8	1.4-2.2 nm	1.8 nm
300	2x6	α-Al2O3+	7.0	2.0-2.5	2.4
525a	2x6	α-Al2O3	5	3.0	3.2
480d	2x6	α-Al2O3	3	3.4	3.4
800a	2x6	a-Al2O3	5	3.0	2.4-4.6
300 K	1x3	C	9.5x10(+12) cm(-2)	0.4-0.8 nm	NA
300	2x3	C	10	0.7-1.0	0.85
300	3x3	C	9	0.9-1.6	
300	4x3	C	9	1.2-1.9	
480d	3x3	C	3	4.0	1.7

carbon support at two objective focus settings.

Fig. 8 : 6 min deposition of Pd at RT on amorphous (a) and on single crystal (b) alumina film support.

Fig. 9 : Pd depositions of 1x3 min (a), 2x3 min (b), 3x3 min (c), and 4x3 min (d) on amorphous carbon at RT.

Fig. 10 : Diffraction intensity profiles of 4 cumulative Pd depositions on amorphous carbon at RT.

Fig. 11 : Diffraction profiles of cumulative Pd depositions on a-Al2O3 and on γ-Al2O3 at RT.

Fig. 12 : 2x6 min Pd depositions at RT on untreated γ-Al2O3 (a), on oxygen plasma treated γ-Al2O3 (b), and on a-Al2O3 (c).

Fig. 13 : Diffraction intensity profiles of 2x6 min Pd deposits on untreated γ-Al2O3 (a) and oxygen treated γ-Al2O3 (b) at RT; on γ-Al2O3 after annealing to 225 C (c) and on a-Al2O3 with subsequent weak beam annealing (d); deposited at 180 C on γ-Al2O3 (e); and of 2x6 min + 1x8 min of Pd deposited on γ-Al2O3 at 180 C (f).

Fig. 14 : Size distribution of Pd particles on γ-Al2O3 deposited and treated at different temperatures.

Fig. 15 : Experimentally measured (1) and Gaussian) diffraction line profiles of Pd on γ-Al2O3 calculated using 3 different peak widths (2 - 4).

Acknowledgements

Thanks are due to Dr. Ch. Park and Fay Marks for contributing their Auger results on the cleaning of alumina surfaces by an oxygen plasma and to Dr. R. Browning for providing the Gaussian peak profile analysis. The work of one of the authors (K. H.) was supported by a NASA Cooperative Agreement # NCC 2 - 283 with ELORET INSTITUTE.

Literature

1. J.F.Hamilton,P.C.Logel,Thin Solid Films 23 (1974) 89

2. H.Poppa,Vacuum - TAIP, in print

3. H.Poppa, Ultramicroscopy 11 (1983) 105

4. P.S.Bagus,C.J.Nelin,C.W.Bauschlicher, 3rd Int.Symp.Small Particles and Inorganic Clusters, Berlin 1984, to be published

5. D.L.Doering,H.Poppa, J.T. Dickinson, J. Catal. 73 (1982) 104

6. K.Heinemann, T. Osaka, H. Poppa, M. Avalos-Borja, J. Catal. 83 (1983) 61

7. M.M.Treacy, T.E.White, Jr., R.A.Della Betta, E.G.Derouane, R.T.K. Baker, edits., ACS Symposium Series 248, Washington D. C. 1984

8. B. V. Johansen, Micron 5 (1974) 209

9. K. Heinemann, M. Avalos, H. Poppa, Proc. 39th EMSA Meeting, Claitor's Publishing Div. 1981, 158

10. C.Park, F.Soria, H. Poppa, Thin Solid Films 116 (1984)

11. J. Metois, K. Heinemann, H. Poppa, Appl.Phys. Letters 29 (1976) 134

12. S. Iijima, Optik 47 (1977) 437

13. H. Poppa, K. Heinemann, Optik 56 (1980) 183

14. S. Ladas, H. Poppa, M. Boudart, Surface Science 102 (1981) 151

15. K.Heinemann, T.Osaka, H. Poppa, Ultramicroscopy 12 (1983) 9

16. P. Gallezot, M. Avalos-Borja, H. Poppa, K. Heinemann, to be published

17. P. Gallezot, Zeolites 2 (1982) 103

18. D.Doering, J.T.Dickinson, H.Poppa, J. Catal. 73 (1982) 104

19. P. Scherrer, Goettinger Nachrichten 2 (1918) 98

20. E. Bauer, Elektronenbeugung, Verlag Moderne Industrie, Muenchen 1958

Table of Contents

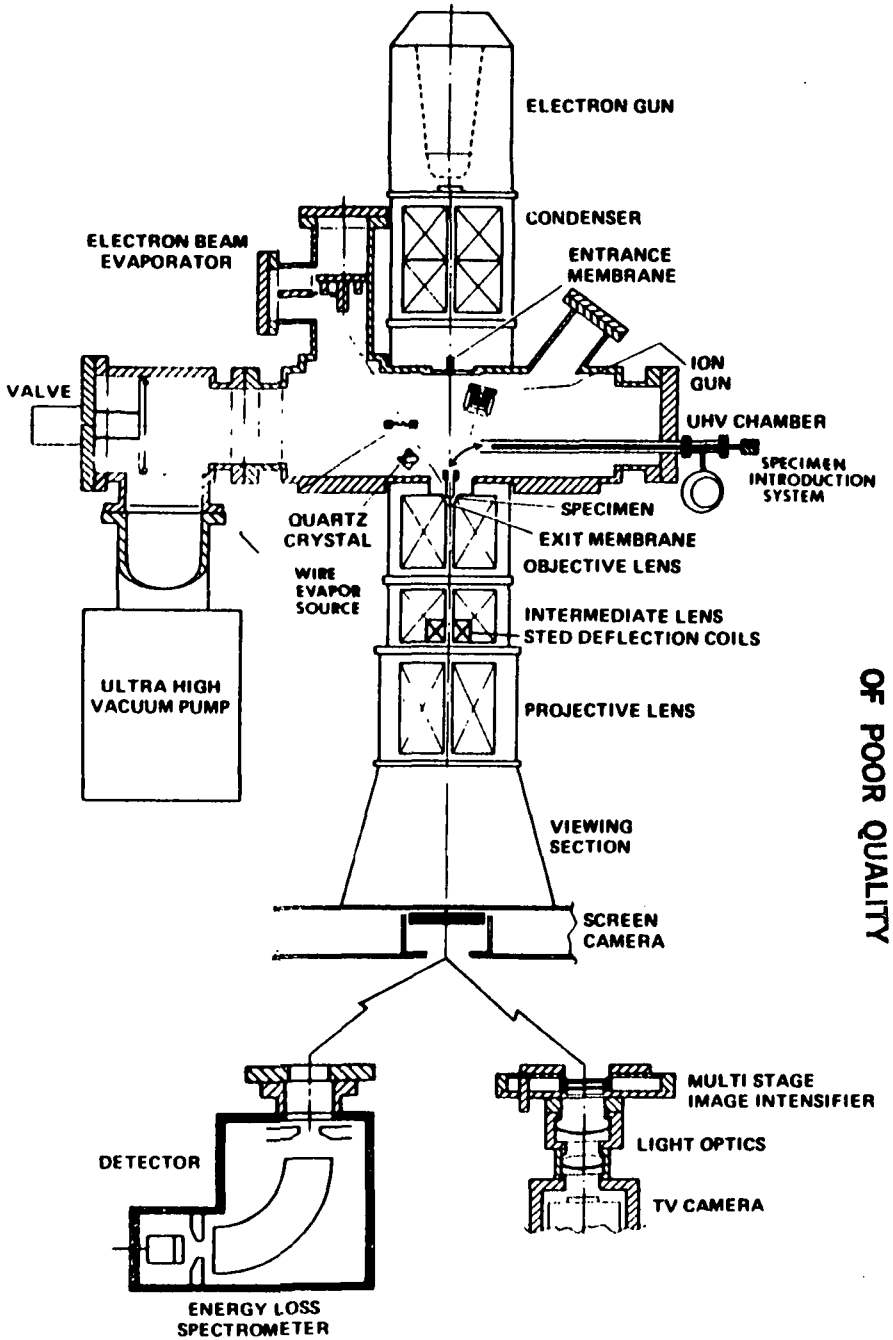

F·g. 1

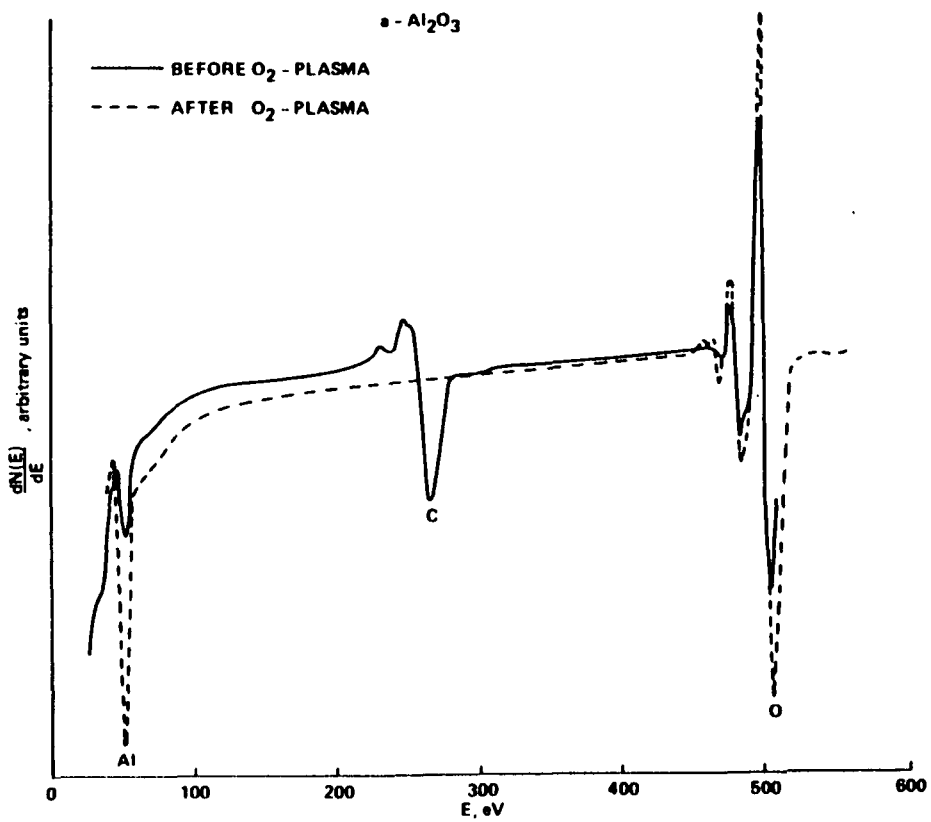

F·g. 2

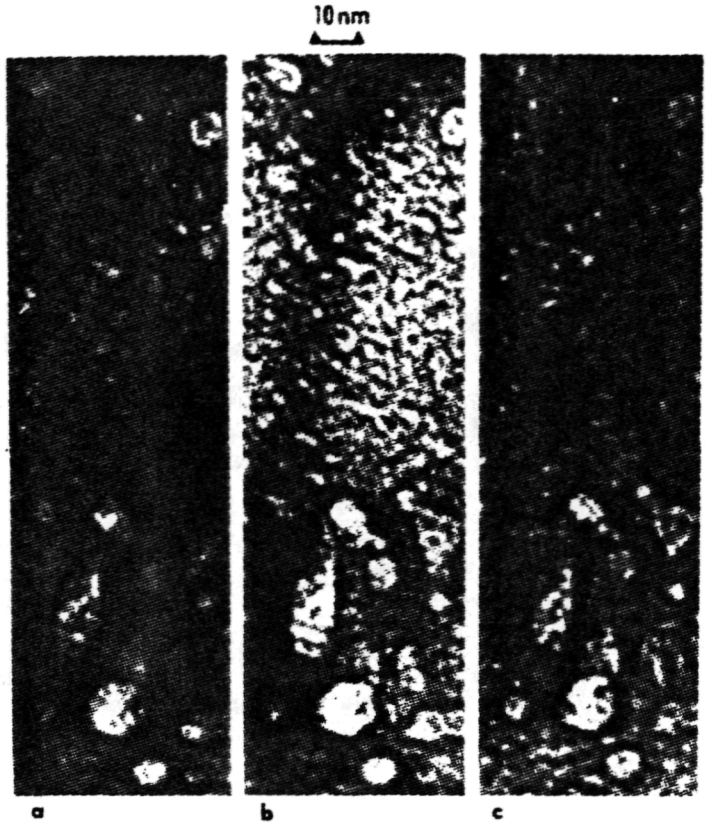

Fig. 3

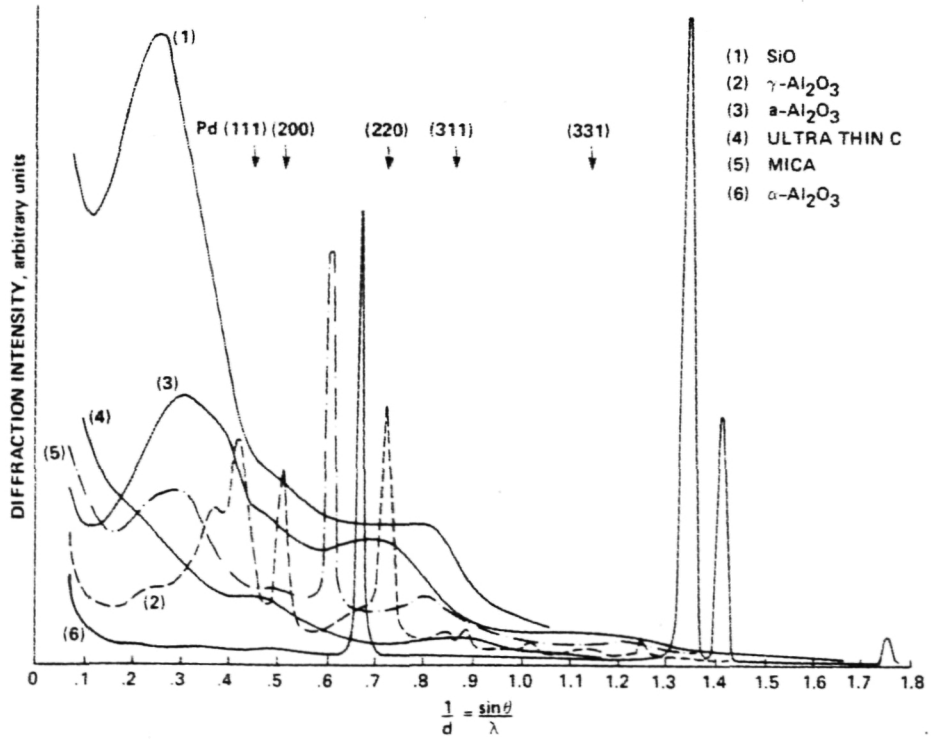

Fig. 5

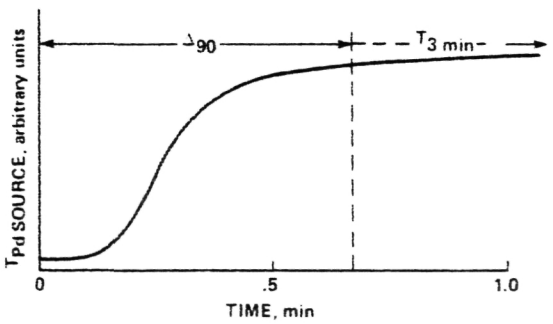

Fig. 6

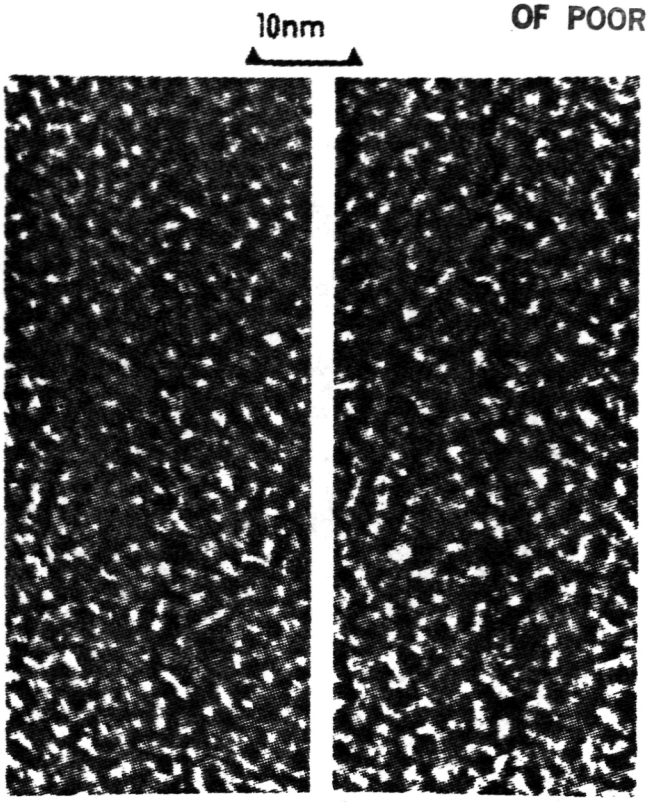

Fig. 7

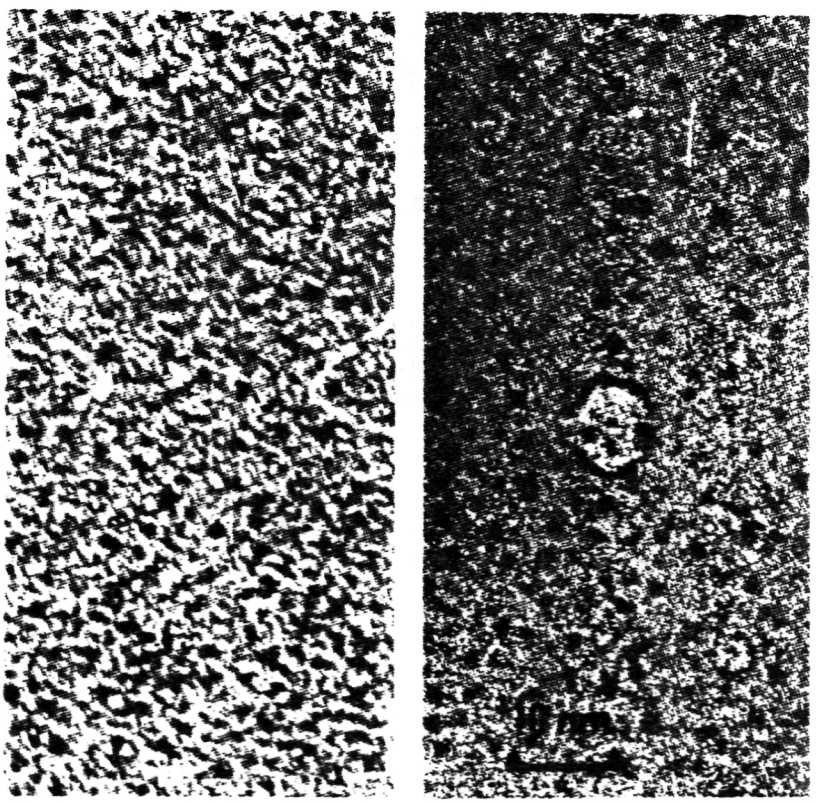

C-2

Fig. 8

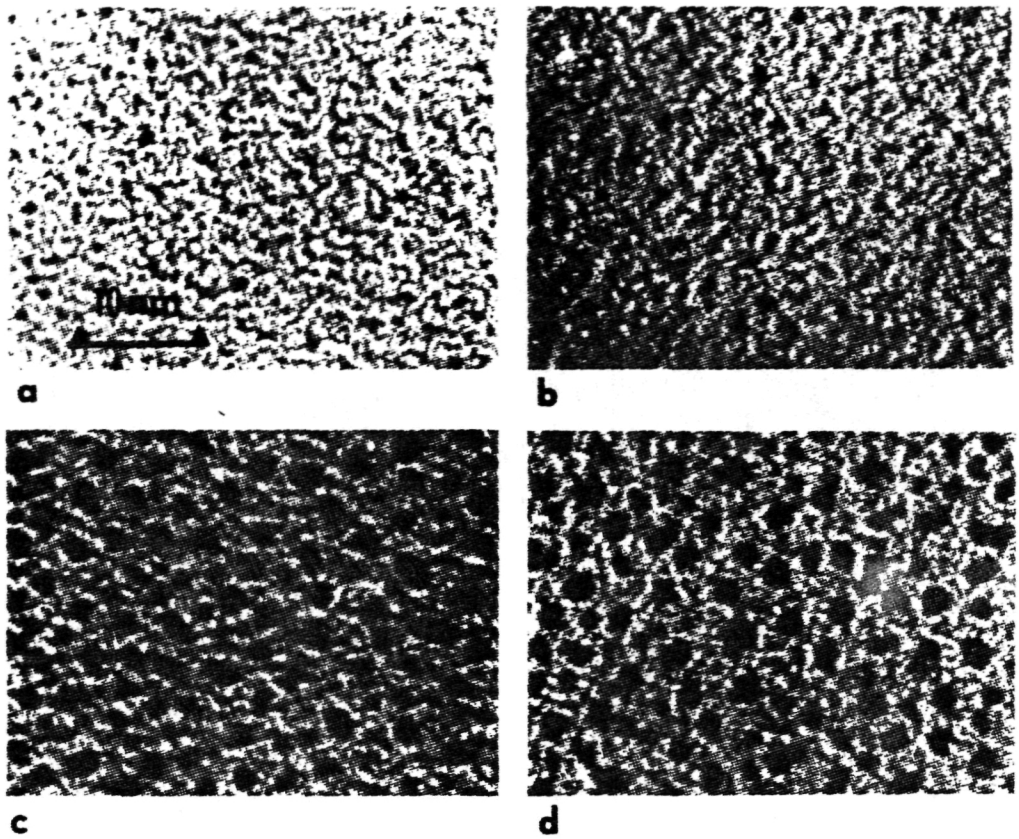
a
b
c
d

Fig. 9

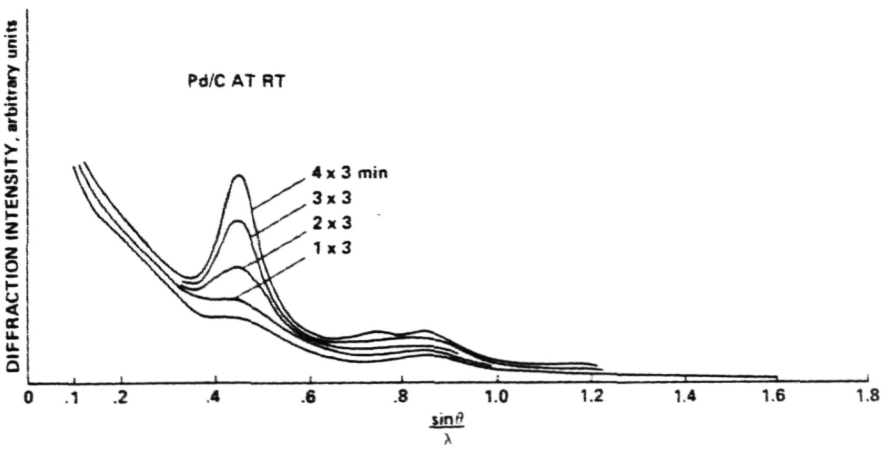
Pd/C AT RT
DIFFRACTION INTENSITY, arbitrary units
4 x 3 min
3 x 3
2 x 3
1 x 3
0
.1
.2
.4
.6
.8
1.0
1.2
1.4
1.6
1.8
sinθ/λ

Fig. 10

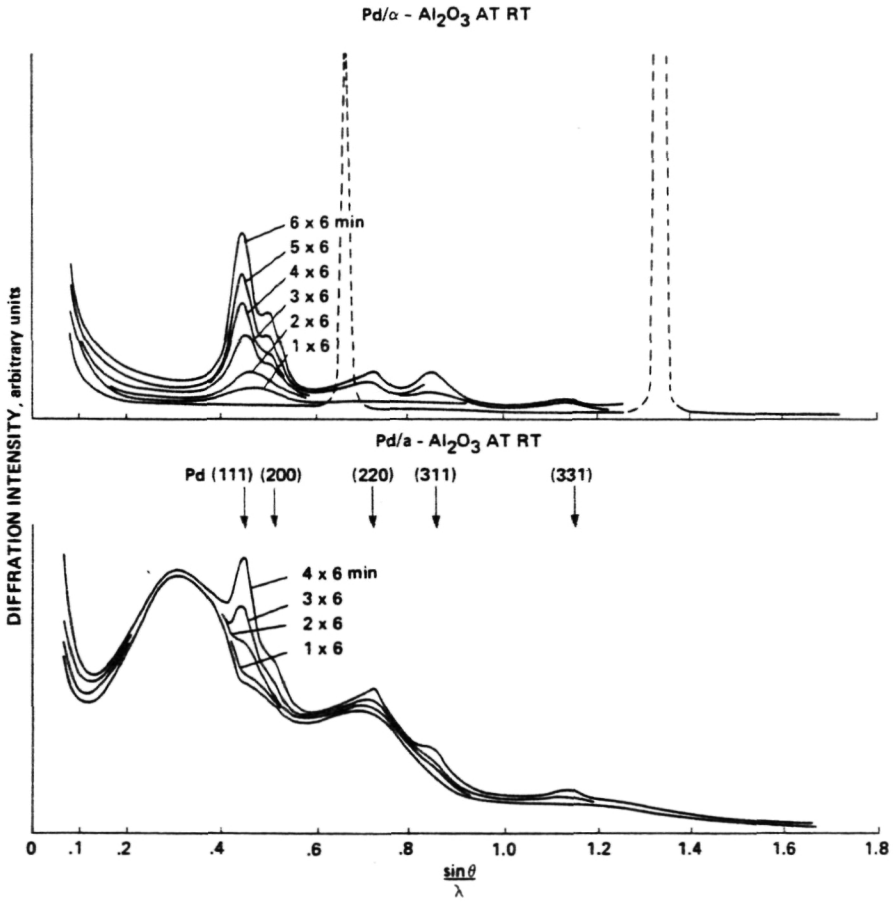
Pd/α - Al2O3 AT RT
6 x 6 min
5 x 6
4 x 6
3 x 6
2 x 6
1 x 6
Pd/a - Al2O3 AT RT
Pd (111) (200)
(220)
(311)
(331)
4 x 6 min
3 x 6
2 x 6
1 x 6
DIFFRATION INTENSITY, arbitrary units
0
.1
.2
.4
.6
.8
1.0
1.2
1.4
1.6
1.8
sin θ / λ

Fig. 11

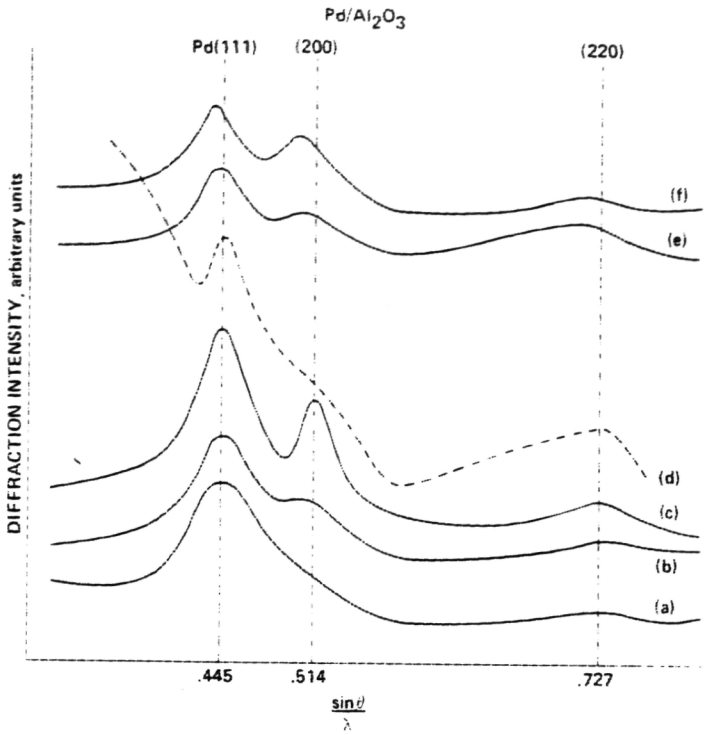

Fig. 13

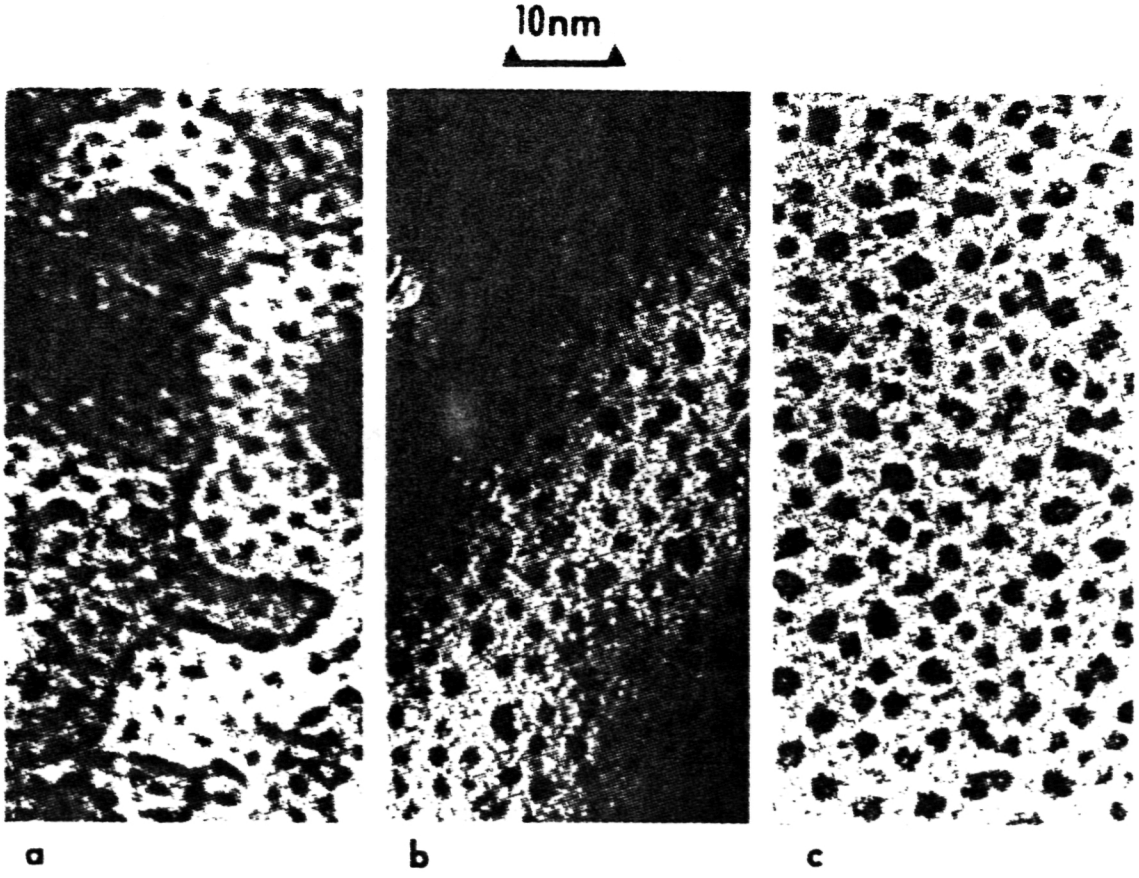

Fig. 12

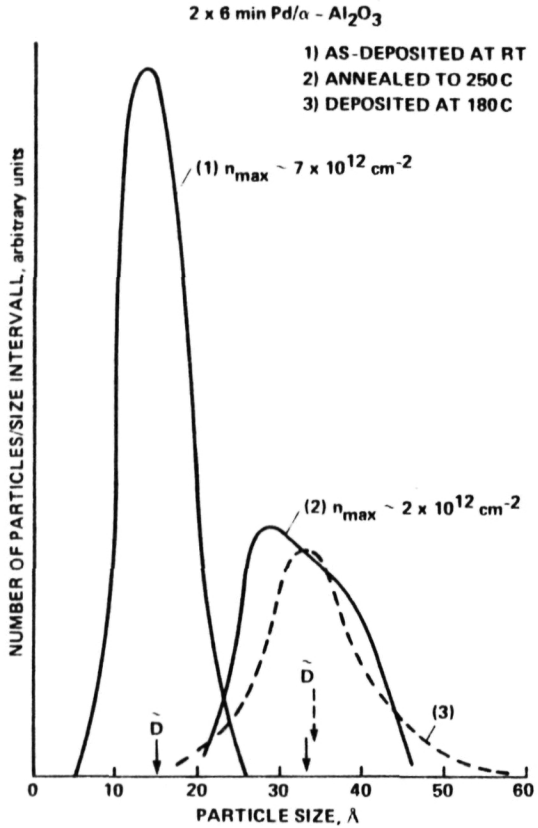
2 x 6 min Pd/α - Al2O3
1) AS-DEPOSITED AT RT
2) ANNEALED TO 250C
3) DEPOSITED AT 180C
(1) nmax ~ 7 x 10^12 cm^-2
(2) nmax ~ 2 x 10^12 cm^-2
(3)
D̄
D̄
NUMBER OF PARTICLES/SIZE INTERVALL, arbitrary units
0
10
20
30
40
50
60
PARTICLE SIZE, Å

Fig. 14

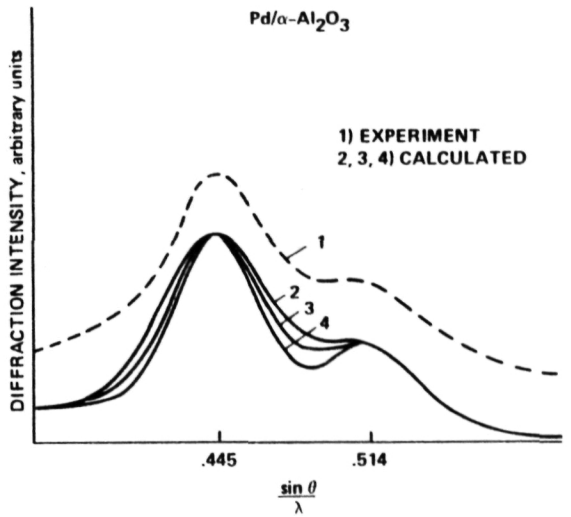
Pd/α-Al2O3
1) EXPERIMENT
2, 3, 4) CALCULATED
DIFFRACTION INTENSITY, arbitrary units
1
2
3
4
.445
.514
sin θ / λ

Fig. 15